Diogo Brízido Caldas Oliveira

Licenciado em Ciências de Engenharia Mecânica

Electron Beam Welding of TZM plates

Dissertação para obtenção do Grau de Mestre
em Engenharia Mecânica

Orientador:Doutora Rosa Maria Mendes Miranda,
Professora Associada com Agregação, Faculdade de
Ciências e Tecnologia da Universidade Nova de Lisboa

Co-orientador: Assoc.Prof. Dr. Norbert Enzinger
Institute of Materials Science and Welding
Graz University of Technology

FACULDADE DE
CIÊNCIAS E TECNOLOGIA
UNIVERSIDADE NOVA DE LISBOA

Setembro 2015

Electron Beam Welding of TZM Plates

Acknowledgments

The research work was accomplished at TU Graz, at the Institute of Materials Science and Welding (IWS).

I cannot thank enough the help I had at IWS, for all that I was taught and for giving me this opportunity. Special gratitude to Prof. Dr. Norbert Enzinger for accepting my proposal, and for his guidance throughout my work. I am extremely grateful to Dipl.-Ing. Markus Stütz for supervising me throughout my daily work in this thesis. For all the productive discussions, suggestions, sharing his knowledge and giving me motivation and inspiration. I want to extend my gratitude to my colleagues at the institute, for making me feel welcome, being always available to help, and especially Dipl.-Ing. Christopher Wiednig for sharing his knowledge. Furthermore, I want to thank the entire team of the institute, the laboratory staff, Leander Herbitschek, Ing. Kurt Kerschbaumer, Gernot Stöfan, Ing. Herbert Penker, and Thomas Friedl, who introduced me to the lab's equipment and always advised me during the experimental part of my work. I am also extremely grateful for Prof. Doutora Rosa Miranda as coordinator of this research, and the support provided to accomplish this thesis.

Finally, I want to express my gratitude and dedicate this thesis to my mother, uncle and brother for their support during my academic years and my stay in Graz. To my friends Alexandre Carvalho, João Noruegas and especially my girlfriend Sofia Branco, without whom I would not be able to fulfil this achievement.

Abstract

Recently, many efforts have been made to join molybdenum and its alloys, such as TZM, due to their interest for industrial applications. However, it has a poor weldability due to high thermal conductivity and high melting temperature, sensitivity to gas impurities and lack of solid state transformations leading to coarse grain formation. Electron beam welding (EBW) is a high energy density process, and welding TZM can result in a smaller fusion and heat affected zones. The aim of this study was to perform an exploratory investigation on the ability of EBW to weld TZM, focusing on the major process parameters, the clamping system and evaluate the effect on the weld tensile strength. The selection of the parameter values and their refinement was performed using design of experiments. Sound welds were obtained, free of pores, cracks and misalignments. A dedicated clamping system was designed, manufactured, and proved to be of major importance. Tensile strength was close to 80 % of the base material, which is remarkably good for this alloy. Pre- and post-weld treatment had no significant effect on the welding strength. However, further work is needed to minimize grain coarsening, eventually by stirring the molten pool using beam deflection.

Keywords: Electron Beam Welding; Molybdenum; TZM Alloy; Design of Experiments; Preheating; Post weld heat treatment

Resumo

Recentemente têm sido conduzidos trabalhos de investigação visando soldar molibdénio e suas ligas, (p.e. TZM) dada a sua importância industrial. Contudo a soldabilidade destas ligas é difícil devido à elevada condutividade térmica, temperatura de fusão, ausência de transformação de fase em estado sólido que resulta na coalescência de grão e possibilidade de reacção com gazes. A soldadura por feixe de electrões, enquanto processo de elevada densidade de energia, permite obter zonas fundidas e termicamente afectadas reduzidas. Este estudo visou explorar as potencialidades da soldadura por feixe de electrões da liga TZM, incidindo nos principais parâmetros do processo e o seu efeito na resistência mecânica das juntas. Foi projectado e fabricado um sistema de fixação que se revelou bastante eficaz. A selecção dos parâmetros foi feita com um software de desenho de experiências. Obtiveram-se soldaduras de boa qualidade isentas de poros, fissuras e desalinhamentos. A resistência à tracção foi cerca de 80% da do material base, o que é um resultado muito bom para esta liga. O pré-aquecimento e o tratamento térmico após soldadura, revelaram não ter influência nos resultados. No entanto, é necessário realizar um trabalho de investigação futuro, de modo a minimizar a coalescência de grão, eventualmente através do uso da deflexão do feixe.

Palavras-chave: Soldadura por Feixe de Electrões; Molibdénio; TZM; Design of Experiments; Pré aquecimento; Tratamento térmico após soldadura

Contents

List of Figures

List of Tables

List of Symbols

0.1 Latin Symbols

A_f	Focus distance
E	Energy Input per Length
I	Beam current
P	Beam power
U	Accelerating voltage
v	Welding speed
v_i	Initial welding speed
v_f	Final welding speed
x_i	Initial welding point
x_f	Final welding point

Greek Symbols

σ	Standart deviation

Abbreviations

DoE	Design of Experiments
DBTT	Ductil to Brittle Transition Temperature
EB	Electron Beam
EBW	Electron Beam Welding
FFD	Full Factorial Design
FZ	Fusion Zone
GTAW	Gas Tungsten Arc Welding
GS	Grain Size
HV	Hardness Vickers
HAZ	Heat Affected Zone
LOM	Light Optical Microscopy
PWHT	Post Weld Heat Treatment
PH	Preheating
RT	Room Temperature
TIG	Tungsten Inert Gas
UTS	Ultimate Tensile Strength
bcc	Body-centered cubic

Chapter 1

Introduction

This chapter explains the background and motivation behind this research. Furthermore, the objectives as well as an overview of the content is given.

1.1 Motivation

Refractory metals such as molybdenum are used in components for several high tech industries due to their unique properties, like high melting point, creep resistance and preservation of their mechanical properties at elevated temperatures. Molybdenum and molybdenum alloys, like the widespread titanium-zirconium-molybdenum alloy TZM, are considered to be attractive structural materials for high temperature applications. Joining can be achieved by conventional mechanical methods e.g. riveting and fastening as well as by advanced brazing and welding techniques. However, developing dedicated joining technologies poses a challenge for the industrial applications of these special materials. Due to the high thermal conductivity and melting temperature, lack of lattice transformation which results in a coarse grain formation and the sensitivity to gas impurities, the toughness and strength of the welded joint is not easy to ensure. Some success was obtained with tungsten inert gas (TIG), electron beam welding (EBW) and laser beam welding, but with considerable embrittlement of the fusion zone and heat affected zone. Nevertheless, with the high energy density from electron beam welding , using adequate process parameters and heat treatment, the negative effects of welding can be reduced.

1.2 Objectives

The purpose of this study was to conduct an exploratory experimental investigation of EBW of 2 mm TZM plates, with a butt joint without filler material. With the aid of Design of Experiment (DoE), the influence of the welding parameters and their interactions on the final weld quality and mechanical properties was defined. A characterization of the weld, through mechanical testing, hardness testing and metallographic analysis was made as well as a clear understanding of the influence from pre- and post-weld heat treatment processes. A systematic investigation and refining of the most relevant parameters allowed identifying the process window of parameters and improving the weld quality.

1.3 Content and structure

This thesis is organized in five chapters. Chapter two presents a critical literature review, on both material and welding technology. The production methods of Mo and Mo alloys were addressed, and a detailed explanation on the alloy TZM properties was given. Electron beam welding process is explained in chapter two as well, with the most important process parameters addressed in detail. In chapter three, a detailed explanation of the experimental procedure is given, organized by chronological order, this chapter lists the welding tests conducted as well as the testing procedures. In chapter four a discussion of the results for each input and output parameter is given, parallel with the statistical analysis provided by the DoE. Finally, a summary and conclusion regarding the information obtained throughout this research is given, together with an outlook of future work this field.

Chapter 2

State of the Art

2.1 Molybdenum

Molybdenum is a refractory metal which does not occur naturally as a pure metal on Earth. Instead, molybdenum is produced by powder metallurgy or by a melting route (electron beam or vacuum arc melting). Through a series of processes that initially isolate molybdenum disulphide (MoS_2) from other components in its ore, molybdenum powder is finally obtained, which can be processed into pure molybdenum and Mo-alloys. Powder metallurgy is the most widely used process, since the fine-grained microstructure obtained from this production method results in easier further processing and improved mechanical properties [1]. A schematic flow of the production of powder metallurgy produced semi-finished products is shown in figure 2.1.

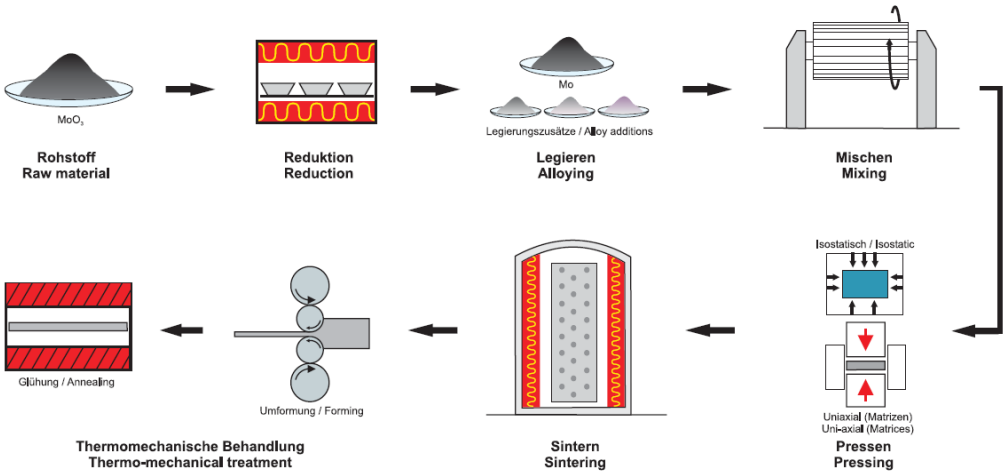

Figure 2.1: Schematic flow of the production of semi-finished products [2].

The most important physical and mechanical properties of pure molybdenum are listed in table 2.1:

Table 2.1: Physical and mechanical properties of Mo.

Crystal structure	bcc
Density	10.28 $^{g}/_{cm^3}$
Melting point	2,620 °C
Boiling point	4,825 °C
Thermal conductivity (20 °C)	138 $^{W}/_{m\,K}$
Specific heat capacity (20 °C)	254 $^{J}/_{kg\,K}$
Young's modulus (20 °C)	329 GPa
Ultimate tensile strength	324 MPa
Fracture elongation	10-15%

Pure molybdenum has poor ductility and a relatively high ductile-brittle transition temperature (DBTT). Contrary to most metals, the recrystallization of molybdenum leads to embrittlement due to precipitations of impurities on the grain boundaries [3].

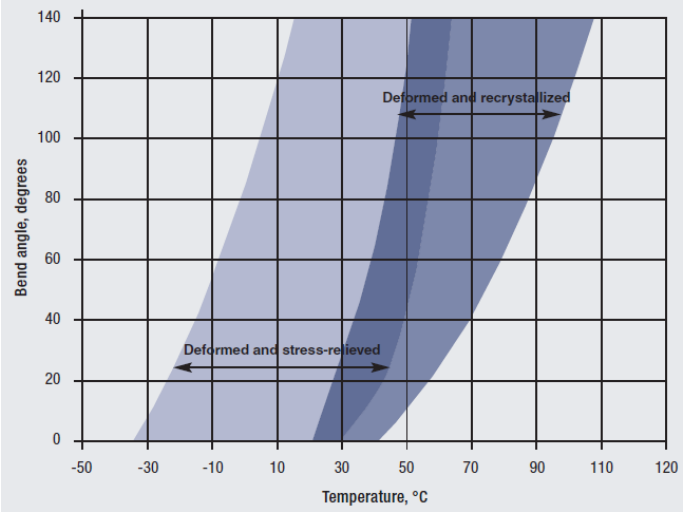

Figure 2.2: DBTT behaviour of sheet metal in deformed and stress-relieved condition and deformed and recrystallized resulting from a three point bend test [1].

Heating molybdenum and its alloys above their recrystallization temperatures results in grain coarsening, which is associated with a reduction in strength and hardness. The recrystallization temperature of molybdenum is strongly dependent on the degree of deformation of the material and its chemical composition.

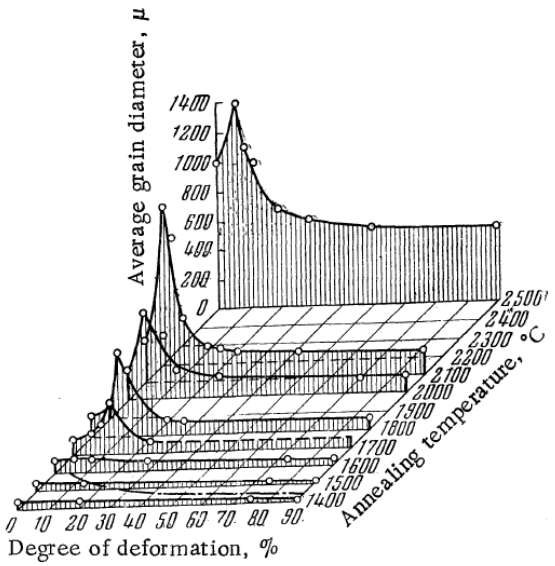

Figure 2.3: Recrystallization diagram of molybdenum [4].

Applications

The first molybdenum metal applications were related to their stability and strength at elevated temperatures dating back to 1910 in the form of wire filament supports in incandescent lamps. Since then, scientists and engineers have discovered that other properties of molybdenum, including high thermal and electrical conductivity, low coefficient of thermal expansion, resistance to attack by molten metal, thermal shock resistance and high stiffness, make it the material of choice for many applications [1].
Due to these properties, molybdenum started to play an important role in electrical and electronic devices such as semiconductor diodes found in consumer products, high-power semiconductor heat sinks used in applications like motor controls, industrial equipment and electrical power generation, thin films transistors (TFT-LCD) displays, and solar cells. In medical equipment, molybdenum components are used for the operation of X-ray tubes used in computerized axial tomography (CAT) scanning equipment. In high-temperature processing, molybdenum alloy tools forge super alloys in the temperature regime above 1,100 °C. Molybdenum alloys are ideal for brass extrusion tools, molten metal casting, liquid metal handling, plastic injection moulding, glass handling equipment and high temperature furnace shields and tooling as demonstrated in figure 2.4. Finally, pure molybdenum finds application as a spray coating on components for automotive and aerospace industries due to its wear resistance.

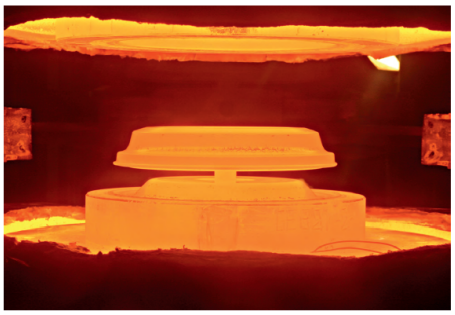

Figure 2.4: Isothermal forging of superalloy turbine discs using TZM alloy tooling [1].

2.2 Molybdenum alloys

In general, molybdenum alloys can be divided into three main types: solid solution strengthening alloys (MoRe); composite metal alloys (MoCu); and carbide strengthening alloys (TZM) [5]. By alloying molybdenum with a small content of a series of elements, properties such as strength, ductility, creep resistance and machinability can be improved considerably [2]. Considering that a higher alloy content leads to an increase in resistance to deformation and DBTT, the maximum quantity of alloying elements is limited to tenths of a percent, thus sustaining the technological ductility. Finally, oxygen-containing atmospheres cause severe oxidation of Mo and Mo-based alloys above 400 °C [2].

Main Alloying Elements

Rhenium, tungsten, tantalum or niobium are used to enhance Mo's properties, most commonly in solid solution strengthening alloys, where this elements replace some of molybdenum's lattice positions. Alloying Rhenium reduces the DBTT resulting in increased ductility[2, 6].
By blending powder prior to sintering, composite metal alloys can be produced by combinations with copper, titanium or sodium. MoCu is a composite material with 30 wt% in copper, characterized by a high thermal conductivity and low thermal expansion.
Alloying additions of boron and silicon results in an increased hardness both at room and elevated temperatures. While a low content of titanium, zirconium, niobium, tantalum and vanadium resulted in some reduction in hardness attributed to the deoxidizing action of these elements, the recrystallization temperature is increased by a few hundred degrees.[4]. Since oxygen and nitrogen are detrimental interstitial impurities, causing grain boundary embrittlement, carbon segregation and precipitation were found to diminish the O_2 segregation, hence promoting ductile behaviour [7].

2.2.1 TZM alloy

TZM is a carbide strengthening molybdenum based alloy, and the chemical composition is stated in table 2.2. Due to both solid solution and precipitation strengthening, the alloy's tensile and creep properties at high temperatures are increased [1, 8].

Table 2.2: Chemical Compostion of TZM alloy.

Element	Content
Molybdenum, Mo	balance
Titanium, Ti	0.5 wt.%
Zirconium, Zr	0.08 wt.%
Carbon, C	0.01 wt.%

The ultimate tensile strength (UTS) of TZM is higher than for pure Mo and decreases similarly with temperature, as shown in figure 2.5. The addition of Zr forms a limited Mo-Zr solid solution, which increases the tensile strength [9] by obstructing grain growth hindering recrystallization and elevating the recrystallization temperature from pure molybdenum's 1,100 °C to 1,400 °C [1, 10, 11]
The grain boundaries of molybdenum are intrinsically weak and carbon atoms compete with other interstitials to reduce the segregation of harmful impurities and to strengthen intergranular cohesion [12].

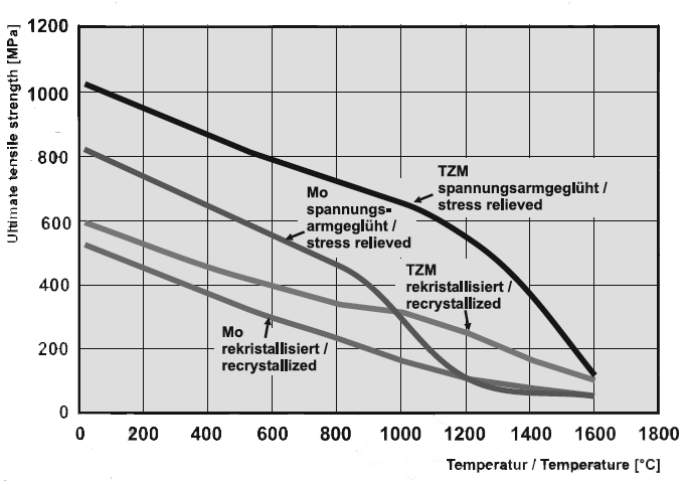

Figure 2.5: Typical UTS strength for Mo and TZM sheet material in the stress relieved and recrystalized condition [2].

2.3 Welding of Mo and its alloys

Refractory metals generally exhibit limited weldability. The main issues associated with fusion welding of Mo and Mo based alloys are the embrittlement of the weldments due to impurities and the grain growth in the heat affected zone(HAZ). The impurities can be introduced by insufficient weld preparation or O and N contamination from the welding atmosphere [13, 14]. Since the toughness and strength of welded joints are not easy to ensure by traditional technologies, EBW of Mo and Mo based alloys has been tested with some success. With its narrow weld and heat-affected zone, electron beam welds are less prone to fail than gas tungsten arc welds (GTAW) with large amounts of heat deposited in the workpiece [5]. Although EBW under vacuum can restrain the harmful effects of O and N [5] and it's highly concentrated low energy input can decrease the occurrence of pores and cracks. Porosity is an important issue in the fusion welding of TZM. Gas porosity cannot be avoided in the weld zone even by using EB welding under high vacuum since, due to the reactive elements in TZM, sheet material typically exhibits oxygen levels of 250 ppm [15]

Fusion welding of Mo-based alloys was investigated in [15]. Electron beam welding butt joints were performed in TZM, Mo41Re alloy and commercially pure Mo in 2 mm sheet format. Figure 2.6 shows the tensile test results of these experiments.

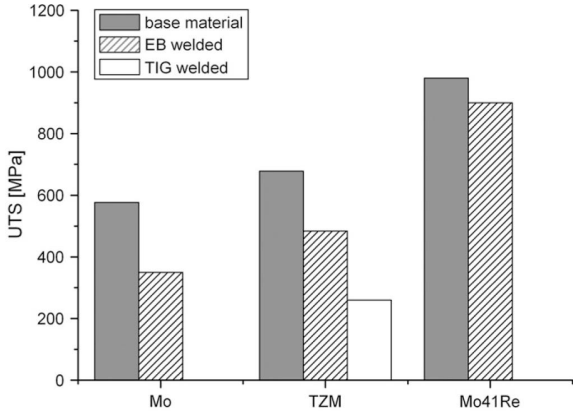

Figure 2.6: Ultimate tensile strength of welded Mo-based materials [15].

For all investigations, welding resulted in a decrease of strength in the weldments. The lowest results were obtained for commercially pure Mo due to grain growth in the heat affected zone and in the fusion zone. TZM showed better joint efficiency as the grain coarsening in the weld zone was reduced compared to unalloyed Mo. TIG welding was also performed on TZM for comparison and showed a wider HAZ which decreased the joint efficiency by 40%. The best results were obtained with Mo41Re, where 90% of the base material strength was maintained [15]. Finally, it is reported that ductile welds were

realised in the Mo41Re material, which can be recommended for application in highly stressed components [15].

EBW and GTAW were conducted in thin molybdenum sheets [16]. Samples were welded with fillet lap joint and through-welded lap joint in 0.2 mm sheets with constant accelerating voltage U = 60 kV,beam current I = 6 mA and welding speed v = 10 mm/s. Experiments proved that EBW produced better welding results in thin Mo sheets compared to GTAW, since it is processed in vacuum and has a much lower heat input. The heat affected zone width of EBW was 1.4 mm compared to 35 mm for GTAW, which is a remarkable difference.

Nevertheless, grain growth in the heat affected zone and a course grained weld fusion zone structure were always observed, as shown in figure 2.7

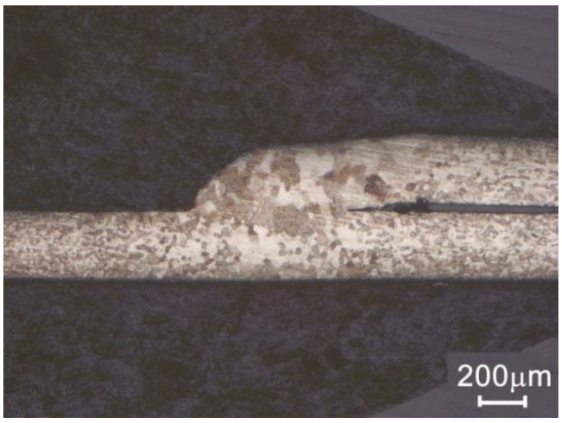

Figure 2.7: Cross section of a EBW Mo-Mo joint [16].

Pre-heating and Post-weld Heat treatment

As large internal stresses can develop in the welding zone, it is advisable to pre-heat the components [2]. Pre-heating above the DBTT minimizes the risk of cracking [15].
Stress-relief annealing after welding was found to be effective, enhancing cohesion of grain boundaries, resulting in increased ductility [12]. The standard stress-relief annealing process is conducted at 1,500 °C inside a high vacuum furnace [17] to prevent embrittlement by gas impurities.

2.4 Electron Beam Welding (EBW)

Electron Beam Welding is a fusion welding process where heat is generated through the impact of an electron beam with high kinetic energy onto the material. Figure 2.8 is a schematic representation of the EBW machine. The cathode is heated to a certaint temperature where a cloud of electrons is formed. These electrons are accelerated by a electric field generated between cathode and anode and finally the electron beam is focused through a series of magnetic coils.
EBW can be processed under high vacuum, medium vacuum and atmospheric pressure. High vacuum allows a higher depth of penetration resulting in a thinner weld bead and ensuring a better purity of the welded metal. When compared to other fusion welding processes, EBW has a number of advantages such as low heat input, narrow fusion zone, deep penetration welds, good weld control and repeatability, high purity and often filler material is not required. The main disadvantages are related to equipment cost, vacuum maintenance and chamber size which limit the component size. Additionally, being a high precision welding process, joints have to be well prepared to guarantee perfect fitting.

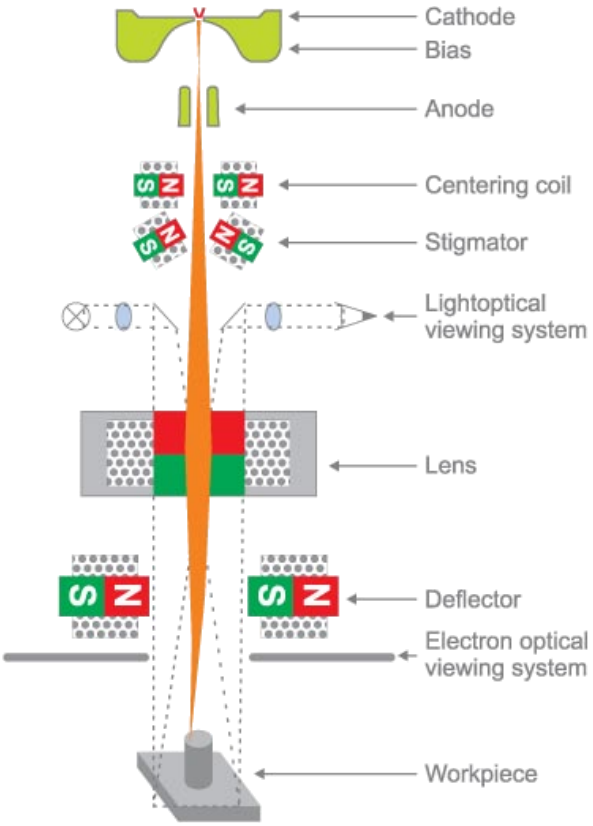

Figure 2.8: EBW schematic [18].

The highly focused and energy density characteristic of electron beam welding allows a deep welding mode. This consists of a deep penetration of the high power beam that transfers energy into depth creating a metal vapour capillary surrounded by a metal liquid phase(figure 2.9 and figure 2.10). Several forces act on this metal vapour capillary , namemly: vapour pressure, gravity, surface tension, hydrostatic pressure. Through the balance of these forces, a keyhole like shape is formed and has to be maintained stable during the welding process to ensure a regular full penetration weld. A rapid solidification occurs in the rear part of the keyhole by epitaxy on the liquid metal interface.

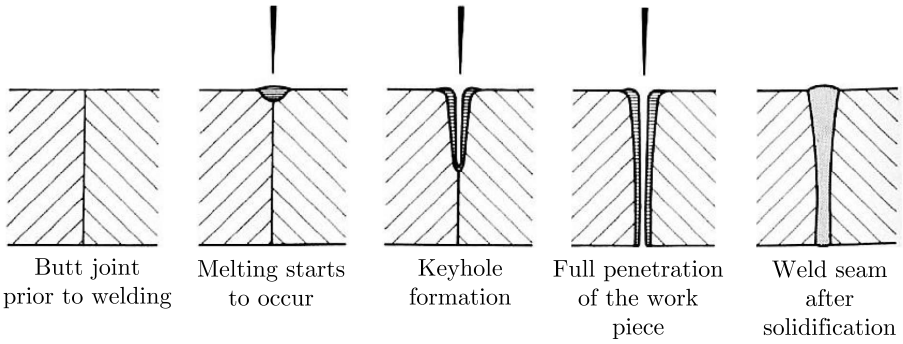

Figure 2.9: Stages of the deep welding effect [19].

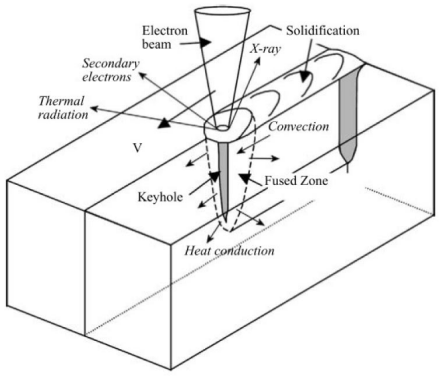

Figure 2.10: Moving keyhole 3D model [20].

2.4.1 EBW Parameters

Electron beam welding is a highly stable and reproducible process in which several parameters play an important role. In this section the most relevant ones will be explained.

Accelerating Voltage (U)

The accelerating voltage is the electrical potential in kilovolts (kV), mainly responsible for the acceleration and speed of the electrons. In order to obtain the smallest beam spot diameter it is advisable to use a higher accelerating voltage and a lower beam current [19]. Therefore, the accelerating voltage is usually kept constant at the highest value available depending on the machine [19] resulting in deeper and thinner weld seams.

Beam Current (I)

The beam current is the measure of the transported charge (e.g. the amount of electrons), usually expressed in milliamperes (mA). The beam current combined with the accelerating voltage results in the beam power and has a large influence in the resulting weld quality. It is a parameter to constantly control and adapt, high enough to obtain full penetration without enabling the material to fall downwards resulting in a concavity on the face of the weld and substantial root size [19].

Focal Distance ($\mathbf{A}_f$) and Lens Current

To focus the electron beam accurately a magnetic lens is used, as shown in figure 2.11. The focusing distance of the lens is related to the current applied to the lens coil. The lens allows focusing the beam into the smallest beam spot on the surface of the material as well as under- or over-focused.

The focal position influences the forces inside the melting pool, the penetration depth as well as the thickness of the weld profile as depicted in figure 2.12. The cross sections from the image below show simultaneously the effect of the accelerating voltage and beam focus. It is an important welding parameter for the process stability, especially for thicker components [19]. For thin plates and high welding speeds the focal position does not have a significant influence [21].

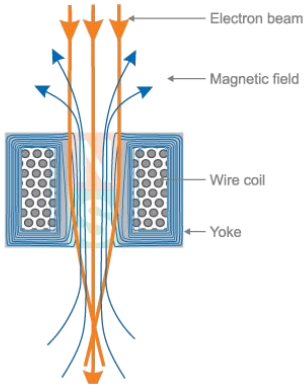

Figure 2.11: Magnetic lens focusing the electron beam [18].

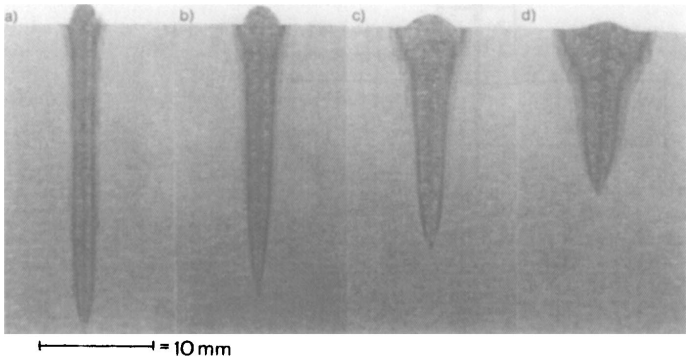

Figure 2.12: Cross sections through welds made with different accelerating voltages and focal distances: (a) U=150 kV, A_f=350 mm; (b) U=60 kV, A_f=350 mm; (c) U=150 kV, A_f=1200 mm; (d) U=60 kV, A_f=1200 mm [19].

Beam Deflection

The electron beam can be deflected by the electromagnetic forces, allowing to control the beam figure, amplitude and frequency of the beam deflection. Deflection and oscillation is useful to beneficially affect the fusion and solidification process, stabilizing the keyhole and finally improving the weld quality [19]. Applying beam oscillation will always develop a thicker weld seam, figure 2.13 shows examples of beam figures and the respective cross section profiles.

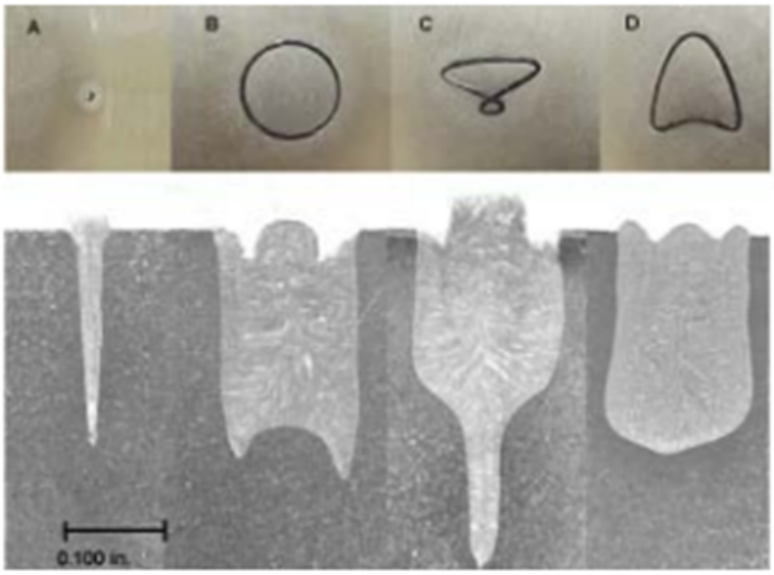

Figure 2.13: Beam Figures and cross sections [22].

Welding Speed (v)

The welding speed is the relative velocity between workpiece and electron beam, measured in mm/s. Together with beam power, the welding speed determines the energy input per length applied into the material affecting the weld depth and thickness [19]. It is a key parameter to be controlled and adapted carefully, since at higher velocities, cracks and pores may occur. Lower values result in a wider weld bead together with a leakage of the melting pool.

2.5 Design Of Experiment (DoE)

Design of Experiment (DoE) is a methodology that allows to organize a set of experiments and determine the cause and effect relationships between input and output variables as well as parameter interactions.
When available material and time are limited, DoE can be used to study several welding parameters simultaneously while consuming resources efficiently. DoE is often preferred over "trial and error" approach, though it still requires a careful plan and selection of both input and output parameters.

2.5.1 DoE Terms

The DoE methodology has two types of variables: *Factors* and *Target Variables*. The factors are the input variables which are adjustable, quantified into *factor-levels*. The target variables are the results of the experiment influenced by the factor-levels and should be quantifiable. After selecting the factors, their respective levels and the resulting target variables, a combination can be arranged using available DoE designs.

2.5.2 Full Factorial Design (FFD)

The full factorial design consists in running experiments at every combination of the factor levels. The number of experiments required is the result of possible combinations. As demonstrated below in figure 2.14 a full factorial design with three factors and two levels requires eight experiments. For this reason, FFD is one of the most error proof designs available [23].

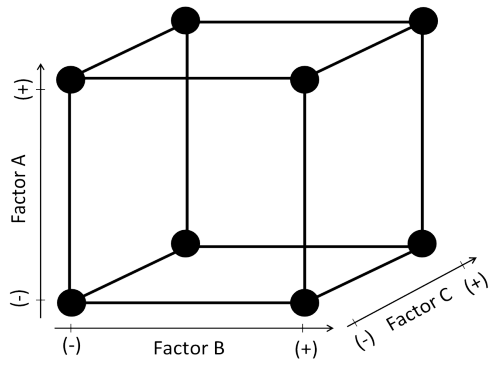

Trial	A	B	C
1	-	-	-
2	+	-	-
3	-	+	-
4	+	+	-
5	-	-	+
6	+	-	+
7	-	+	+
8	+	+	+

Figure 2.14: Full Factorial Design with three factors and two levels.

2.5.3 Analysis

In order to better analyse the information obtained by the design combination, several plots are used. The *Main Effect Plot* displays which parameters have a bigger influence on a specific output variable. This effect is visualized compared to the mean values of the response. As exemplified in figure 2.15(a) parameter B does not affect the response but the remaining parameters do. While the *Main Effect Plot* only shows the individual behaviour of each input parameter, the *Interaction Plot* allows to detect any interaction between parameters. This interaction is present when the lines in the graphic are not parallel as in figure 2.15(b), which shows a clear interaction between parameters B and C.

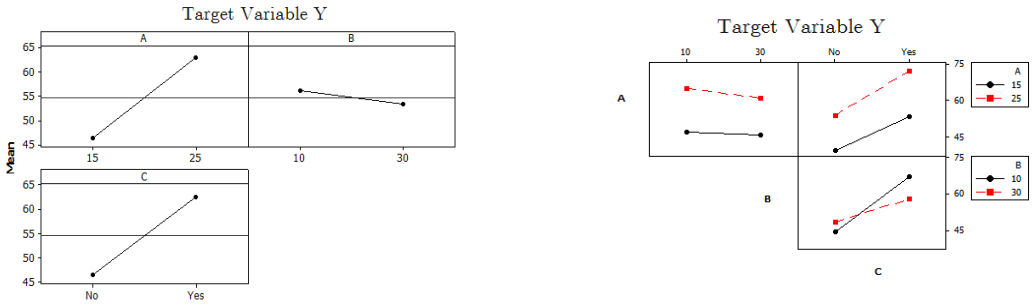

(a) (b)

Figure 2.15: a) Main Effect Plot, b) Interaction Plot.

To understand how a target variable changes depending on two parameters, one of the most effective plots is the *Contour Plot*. The *Contour Plot* displays the development of a response through contour lines with constant values in relation to two input parameters. This plot is very useful to determine the best combination for a certain target value as demonstrated in figure 2.16. The analysis of the experiment is generally determined with software assistance and especially when representing the data graphically. For this thesis, the software Minitab16 was used.

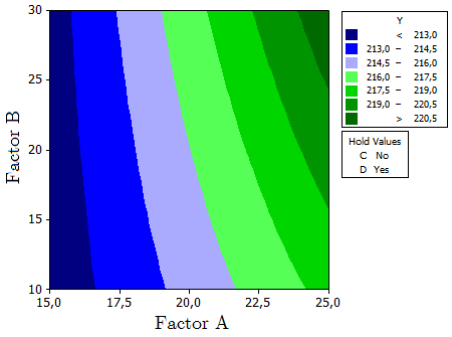

Figure 2.16: Contour Plot.

Chapter 3

Experimental Procedure

3.1 Introduction

This chapter describes the experimental part of the investigation starting with the material and the equipment used. The selection process of the welding parameters is described as well as the welding procedure, the methodology used to evaluate the influence of the parameters on the weld quality and their interactions.
The Pre-Heating process with the Electron Beam is explained and a brief overview on the Post Weld Heat Treatment is given. The last section of this chapter will consist of the explanation of the investigations conducted on the welded specimens.

The following flowchart gives a graphical view on the complete experimental process of this investigation.

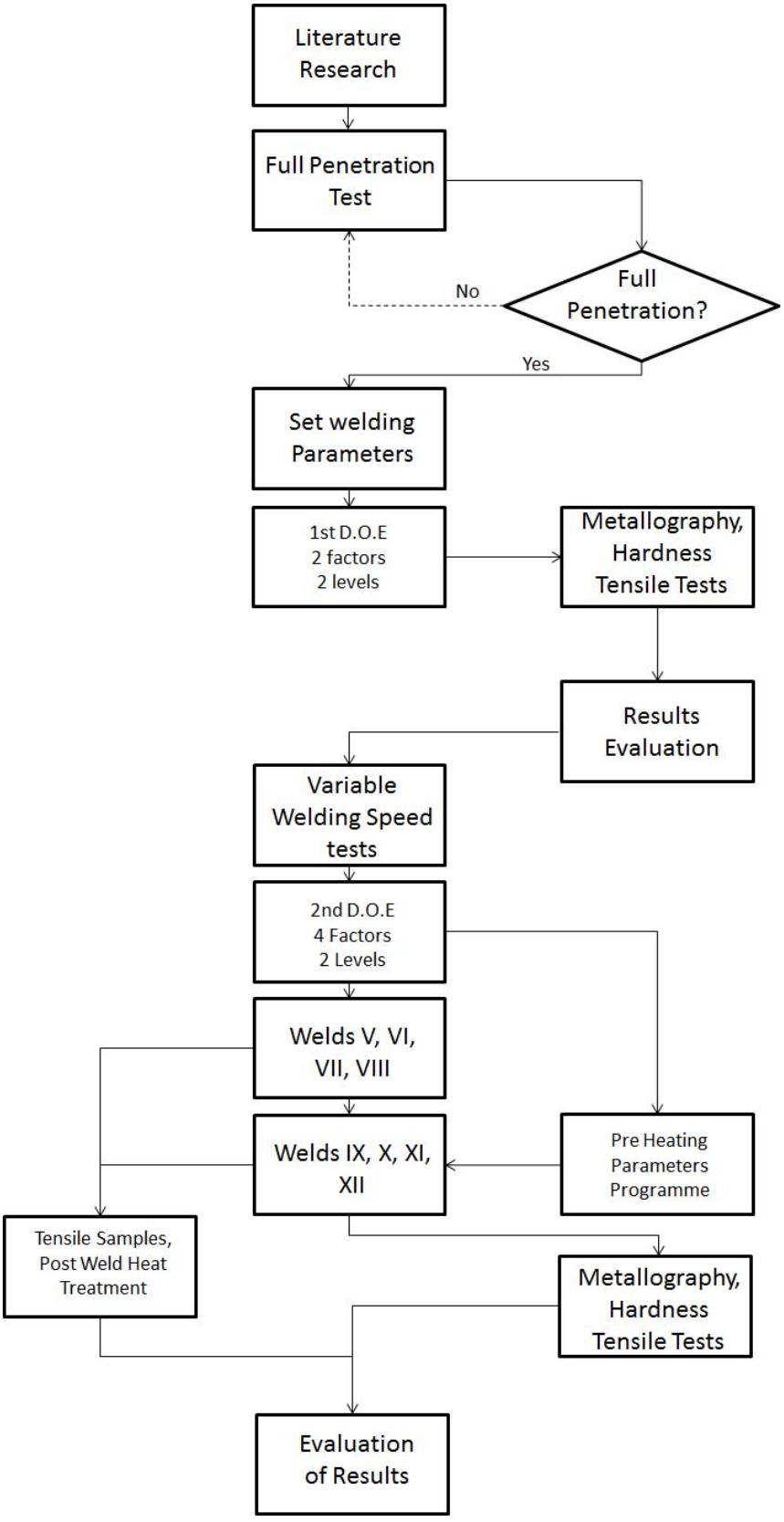

Figure 3.1: Research overview.

3.2 Material

Molybdenum alloy TZM was used in this study. The material was produced by powder metallurgy and the chemical composition is presented in table 3.1. The material was provided by the company Plansee, in plates with 60 mm width, 120 mm length and 2 mm thickness. The microstructure is shown in figure 3.2. It consists of anisotropic grain orientation characteristic of a cold rolled sheet.

Table 3.1: Chemical Compostion of TZM alloy

Element	Content
Molybdenum, Mo	balance
Titanium, Ti	0.5 wt.%
Zirconium, Zr	0,08 wt.%
Carbon, C	0,01 wt.%

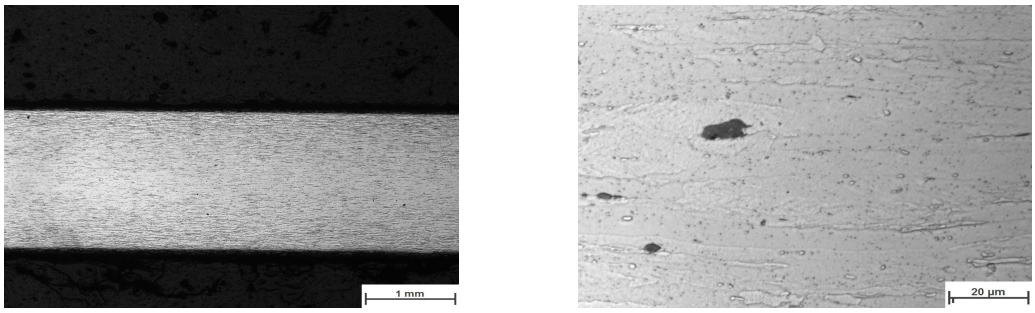

(a) (b)

Figure 3.2: TZM alloy microstructure: (a) low magnification, (b) high magnification.

3.3 Electron Beam Welding Machine

Electron beam welding technique was used to weld the TZM plates under high vacuum with a pressure 8.5×10^{-4} mbar. The EBW machine Kammeranlage EBG 45-150 K14 from *pro-beam* (Figure 3.1) was utilized in the experiments. This machine has a modular beam gun, that can be mounted horizontal or vertically. Offering a wide range of applications, it is especially appropriate for research and prototype welding. Technical specifications are listed in table 3.2.

Table 3.2: *Pro-beam K 14* machine technical specifications.

Max. beam power	45 kW
Max. voltage	150 kV
Max. beam current	300 mA
Chamber volume	$1.4\,m^3$
Operation vacuum directed	$5{\cdot}10^{-4}$ mbar
Beam deflection speed	$1\,°/\mu s$
Min. beam focus	1 mm

Figure 3.3: *pro-beam Kammeranlage K14* electron beam welding machine.

3.4 Welding

For the scope of this investigation, and considering the material available, a selection of the welding parameters was done. This selection intended to apply the Design of Experiments procedure, by focusing on the most relevant parameters while keeping all others constant. From the literature investigation carried out, the beam current and welding speed were the ones that mainly influenced the weld morphology.
A higher accelerating voltage results in a deeper and thinner weld seam which was of interest in this investigation. No further influence on the weld quality was reported, therefore the voltage was kept constant. Since focusing the beam into a point would result in the thinnest seam possible and a key-hole formation assisted by beam oscillation was not required, no other beam figure and oscillation were chosen. The focal position was set on the material surface and kept constant, considering that a variation of the focal position is usually more relevant for thicker specimens [24]. All the welds in this study were cleaned with alcohol prior to welding. A summary of the parameters kept constant

throughout this investigation is listed in table 3.3

Table 3.3: Parameters kept constant.

Parameter	Value
Acceleration Voltage	150 kV
Focal Point	0, surface
Beam figure	Point

3.4.1 Bead on Plate Welding

The goal of the bead on plate welding tests was to have a first practical understanding of the information gathered from the literature research. These tests allowed to visualize and quantify the role of beam current and welding speed on the depth of penetration, and was the basis of the parameter selection for the first full factorial design.
The parameter range is described in table 3.4

Table 3.4: Bead on plate welding parameters.

Weld	Beam Current I (mA)	Welding Speed v (mm/s)
BW 1	20	20
BW 2	10	10

For this, a TZM plate fixed on a steel clamping system was used for both welds, parallel to each other with a small gap in between. The plate was fixed on one of the sides, as shown in figure 3.4. The clamping system can be adjusted and fixed to the working table of the EBW machine. The dotted lines represent both welds.

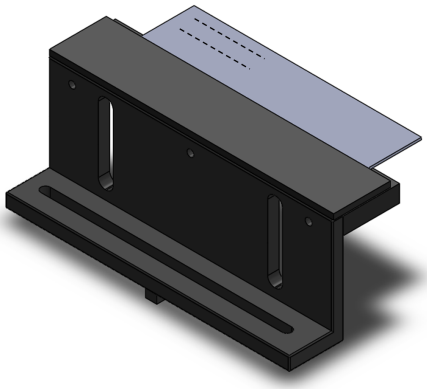

Figure 3.4: Bead on Plate setup.

3.4.2 Two-factor Full Factorial Design

With the results obtained from the bead on plate tests a starting point was chosen, that would guarantee full penetration. From that point, a parameter window was designed for a two factors two levels full factorial design. The factors altered were beam current and welding speed. The output parameters were width, grain size and hardness of both fusion and heat affected zones.
All other parameters were kept constant at the same level as mentioned in the previous section. The factor combination for the parameters is shown on table 3.5

Table 3.5: Factor Combination for the first full factorial design.

Weld	Beam Current I (mA)	Welding Speed v (mm/s)
W I	15	5
W II	25	5
W III	25	15
W IV	15	15

3.4.3 Temperature Measurment

A temperature measurement was set up in order to register the temperature fields during and after the welding process. This was done by spot welding three thermocouples, to the TZM plates at increasing distances from the weld seam. The thermocouples used were type K with a temperature range between 200 °C and 1250 °C. The temperature was measured during welding and kept until the temperature declined to room temperature.
The thermocouples were placed linearly at 5, 10 and 15 mm from the weld seam, as illustrated in figure 3.5

The first measurement was conducted during weld W I, with the welding parameters: $I = 15\,\mathrm{mA}$; $v = 5\,\mathrm{mm/s}$. Although the thermocouples were isolated with a rubber tube and aluminium foil, the electron beam inflicted a big distortion on the thermocouples measurements.
In order to reduce this influence, another measurement was executed using ceramic tubes to isolate the initial part of the thermocouples closer to the seam, while the rubber tubes and aluminium foil isolated the remaining length.This measurement was done during weld W IV with the parameters: $I = 15\,\mathrm{mA}$; $v = 15\,\mathrm{mm/s}$. Further attempts were done to register the temperature profile during welding. Unfortunately, due to the difficulty in

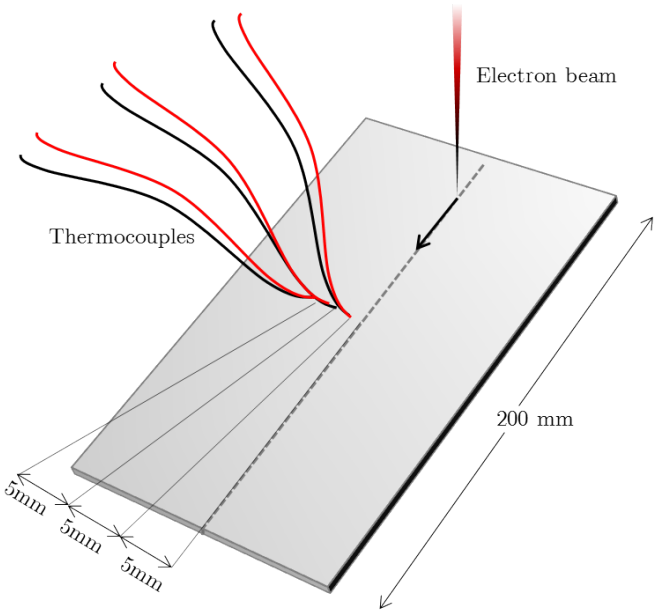

Figure 3.5: Temperature measurement setup.

welding the thermocouples to the plates and the distortions on the measurements caused by the electron beam, a quality measurement of the temperature close to the seam was not possible to acquire.

3.4.4 Variable Welding Speed

From the previous tests, it was possible to establish and understand the relationship between parameters and their influence on the outputs. Before performing a second full factorial design, a small test was conducted to assist in the refinement of the parameters. For these experiments, several bead on plate welds were executed. For each weld the beam current was kept constant, while the velocity changed along the distance. To achieve this variation, a existing variable welding speed program was used. Given the welding parameters, and defining initial and final speed, the program automatically interpolates the data, and executes a linear variation of the velocity along the weld seam. Table 3.6 demonstrates an example of the parameter order being introduced in the code for a weld with 80 mm length with velocity being varied between 30 mm/s and 15 mm/s.

After welding, the velocity at a specific location on the seam can be calculated with a simple linear equation $v = mX + b$ that can be determined using the initial and final welding points (x_i ; v_i) and (x_f ; v_f) as depicted in Figure 3.6.

Table 3.6: Parameter introduction for variable welding speed test.

	y axis(mm)	x axis (mm)	I (mA)	v (mm/s)
Slope In	0	0	0	30
Initial Point	0	(x_i)=5	10	(v_i)=30
Final Point	0	(x_f)=75	10	(v_f)=15
Slope Out	0	80	0	15

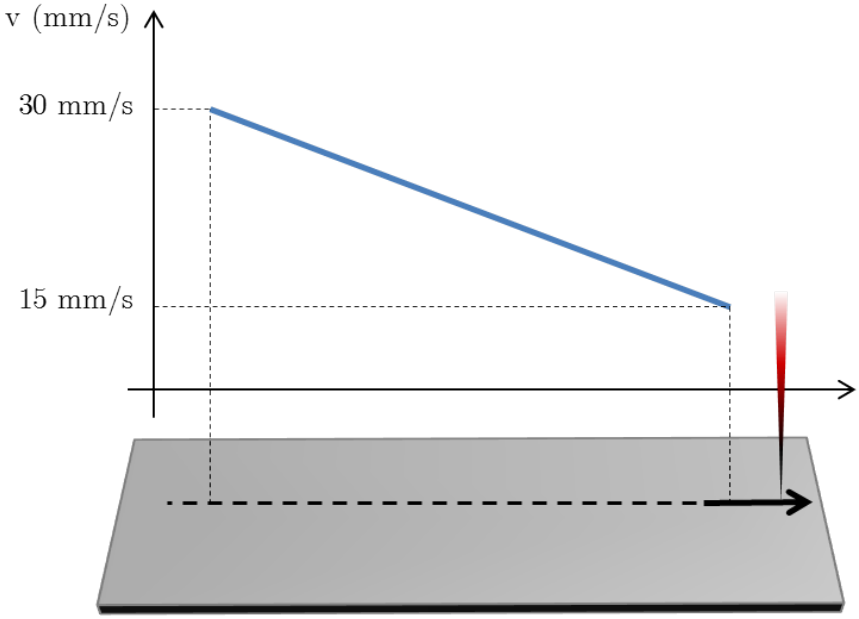

Figure 3.6: Dynamic welding test.

Different currents were chosen, not only to evaluate the relationship between heat input and penetration, but also the quality of weld shape. The bead on plate welds and respective parameters are listed in Table 3.7.

Table 3.7: Variable welding speed test parameters.

Weld	I (mA)	v_i (mm/s)	v_f (mm/s)	E (J/mm)
Dyn I	5	10	2.5	75 - 300
Dyn II	10	20	5	75 - 300
Dyn III	15	30	15	75 - 150

3.4.5 Four-Factor Full Factorial Design

After the preliminary tests and a first analysis of results, a comprehensive factorial design of experiments was done considering four factors (I, v, preheating and post-weld heat treatment) at two levels. This experimental process had four main goals: refine the parameters already studied (I and v), re-evaluate their influence and interactions and finally, evaluate two new factors: preheating (PH) and post weld heat treatment (PWHT). All other parameters were kept constant as defined previously in table 3.3. The factor combination for the parameters is shown on table 3.8.

Table 3.8: Factor Combination for the four-factor full factorial design.

Weld	Beam Current I (mA)	Welding Speed v (mm/s)	PH	PWHT
W V	15	10	No	No
W VI	25	10	No	No
W VII	15	30	No	No
W VIII	25	30	No	No
PH IX	15	10	Yes	No
PH X	25	10	Yes	No
PH XI	15	30	Yes	No
PH XII	25	30	Yes	No
TT-W V	15	10	No	Yes
TT-W VI	25	10	No	Yes
TT-W VII	15	30	No	Yes
TT-W VIII	25	30	No	Yes
TT-PH IX	15	10	Yes	Yes
TT-PH X	25	10	Yes	Yes
TT-PH XI	15	30	Yes	Yes
TT-PH XII	25	30	Yes	Yes

For a FFD with four factors and two levels, 16 trials are required. Given the fact that the last parameter is the PWHT and its effect could only be evaluated through tensile tests, the FFD is achieved by cutting two tensile specimens from each of the eight welds: eight specimens were tested as welded, and the remaining eight after a post weld heat treatment.

As table 3.8 demonstrates, eight welds were executed (represented by "W" and "PH") and the remaining eight rows (represented by "TT") are the tensile tests extracted for PWHT.

Clamping Device

During the previous experiments, all welds were prepared by clamping the two plates separately and aligning them as in figure 3.7. Although this clamping device allows securing plates within a wide range of dimensions, when aligning thin plates such as the ones in this investigation, guaranteeing an uniform alignment was challenging. The process was time consuming and occasionally resulted in an offset of the weld seam.

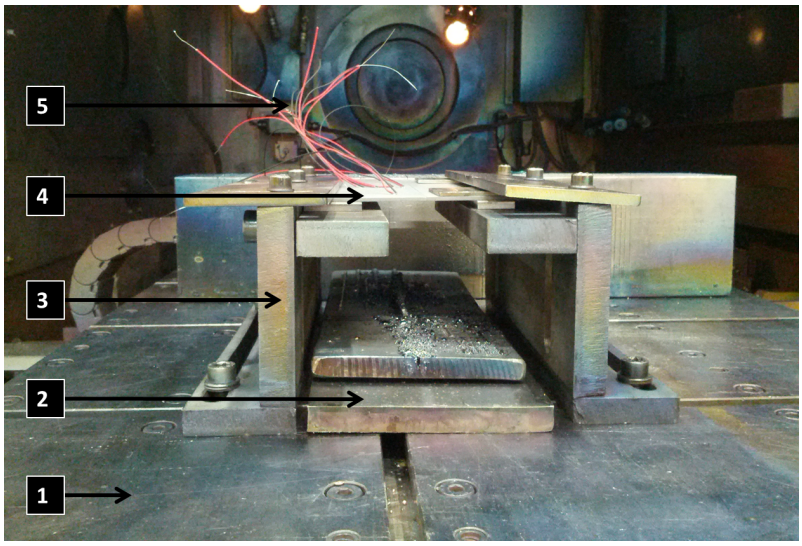

Figure 3.7: Original Clamping System: (1) Motion Feed Table; (2) Backing Plates; (3) Clamping System; (4) TZM Plates; (5) Thermocouples.

To solve this problem, and reduce the preparation time, a new clamping device was designed as in figure 3.8 . It consisted in using two aluminium "L" shaped profiles for each side, with a slot cut in the centre to reduce loss of welding distance. The friction between the TZM plates and the Aluminium clamping was strong enough to endure the forces induced by thermal expansion, and assured an even and constant alignment. Also, the preparation time was highly reduced. A more complex system can be developed specifically for thin plate welding, but this new device was designed to solve the problem quickly and with reduced costs.

When welding with the new clamping device, the aluminium profiles would rest on top of the original clamping system, with enough space underneath to place backing plates. With this setup, the TZM plates were exactly aligned with the height of the copper block inside the chamber, used for adjusting the lens current and focal position. This alignment

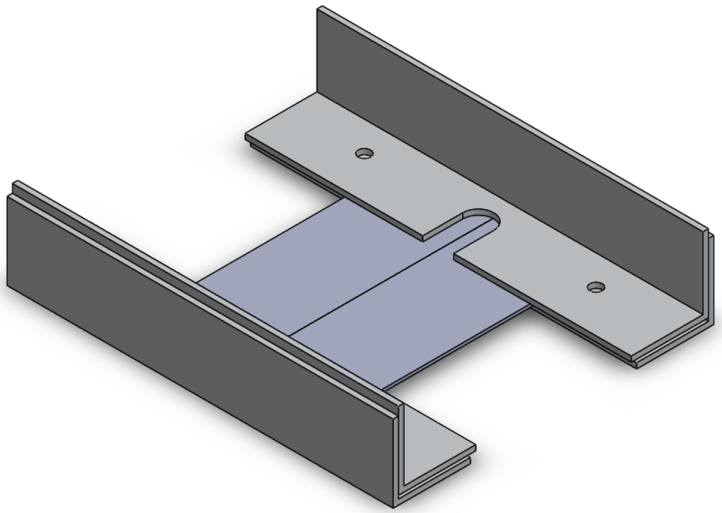

Figure 3.8: Clamping system.

had to be precise and was crucial to guarantee the focus of the beam on the TZM plates surface.

Preheating

Preheating the welds is advisable since high internal stresses can develop due to the welding [2] it can reduce the occurrence of pores and minimize the risk of cracking.
The preheating of the TZM plates was conducted with the EBW machine. This process was thought to be investigated since with the EBW machine, preheating is conducted under high vacuum and so a pure atmosphere allows the temperature to reach a higher range of values. Another advantage was to conduct both heating and welding using the same machine, which reduced operations time so that welding immediately follows preheating.

The first step was to develop a new program code for the EBW machine. This code combined two programs already available: a existing beam deflection program [25] and the standard welding program. The beam deflection program was used for heating, by deflecting the beam into a rectangular beam figure composed by 10 x 100 points. Having both processes done automatically by the machine, without user interaction in between, was very important for two main reasons: reduction of time between preheating and welding and a guaranteed reproducibility of the process for all welds. All the preheating and welding parameters entered and changed in this tests are shown in table 3.9

The program code was tested on a steel plate and to visualize the heating pattern a lower frequency and power were used. Figure 3.9 shows the process steps using screenshots from

Table 3.9: Preheating and welding program parameters

Process	Parameter	Units
Preheating	Beam Current	mA
	Heating Time	s
	Beam Figure dimensions	mm
	Frequency	Hz
	Figure center point	X,Y coorinates
Welding	Beam Current	mA
	Welding Speed	mm/s
	Welding Distance	mm
	Welding Starting Point	X,Y coorinates

a video recording.

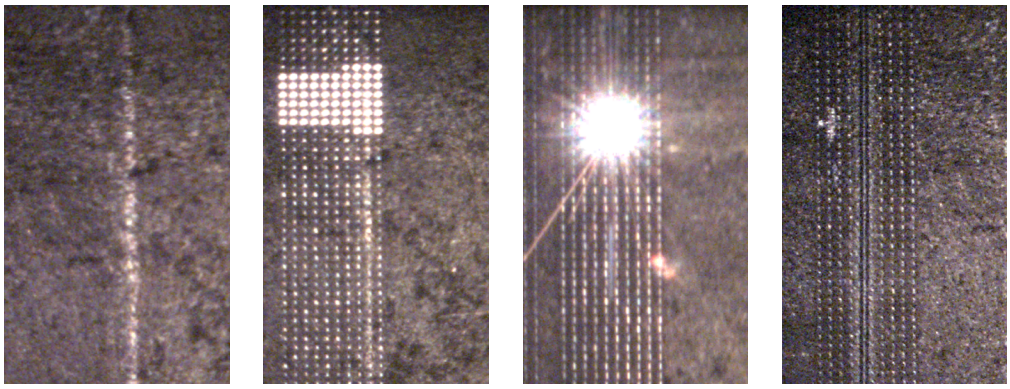

(a) Steel plate (b) Heating (c) Welding (d) Weld seam

Figure 3.9: Electron beam preheating and welding automatic process.

A series of heating tests were conducted on TZM plates. The goal was to find the best set of parameters in order to obtain temperatures close to 400 °C without damaging the surface of the material. From literature research [26] on preheating with electron beam, the first values for the parameters were chosen. Table 3.10 describes the tests conducted on TZM in order to achieve the desired temperature.

Three thermocouples were spot welded onto the plates as in previous experiments in order to measure the temperature profile. To reduce loss of heat through conduction, and protect the aluminium clamping, (10x10x50 mm) steel spacers were placed between the TZM plates and the aluminium profiles.

Table 3.10: Preheating Tests.

Test	Beam Current	Time	Figure Dimensions
T1	10 mA	20 s	12 x 120 mm
T2	10 mA	30 s	12 x 120 mm
T3	15 mA	20 s	12 x 120 mm
T4	15 mA	40 s	12 x 120 mm
T5	15 mA	40 s	40 x 120 mm
T6	15 mA	60 s	40 x 120 mm

Post Weld Heat Treatment

Post weld heat treatment was conducted at 1200 °C for two hours in a vacuum furnace by Plansee .

3.5 Testing

In order to evaluate the welds, a series of tests was done. From each welded plate samples were removed for mechanical and microstructural tests as figure 3.10 shows the layout of specimens in the welded plate.

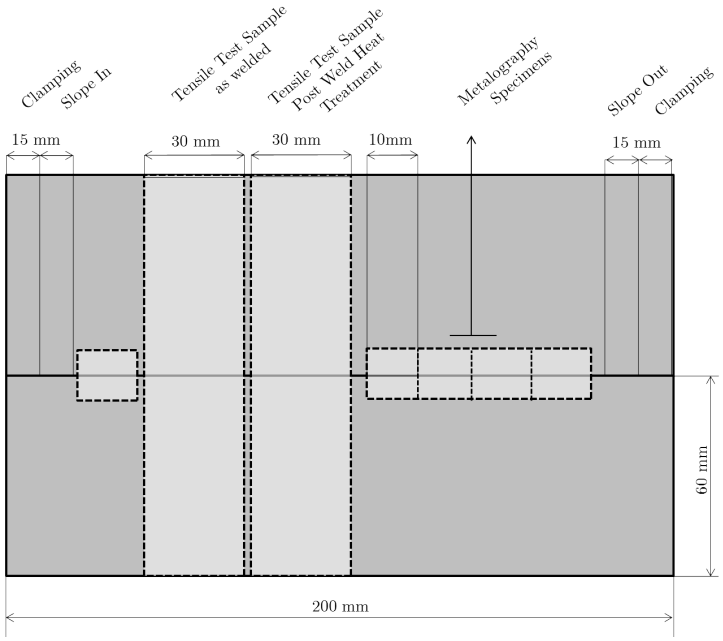

Figure 3.10: Layout of investigation samples.

3.5.1 Microstructure

Analysis of the microstructure, grain size and internal defects was carried out by light optical microscopy (LOM) using a Carl Zeiss Axio Observer. The weld specimens were mechanically cut and mounted in resin. Every specimen was grinded with grit sizes between 320 and 4000, and subsequently polished with 3 μm and 1 μm diamond abrasive paste. The complete process was executed using Struers TegraForce-5. Finally, specimens were etched with Murakami (100 ml H_2O, 10 g K3Fe(CN)6, 10 g KOH) for 30 seconds [17].

3.5.2 Grain Size Measurments

For the grain size measurement procedure, several photos of the microstructure in the fusion zone and heat affected zone were taken, for every weld specimen. The software from Carl Zeiss Vision, Axiovision Grain was used to apply the comparative method of overllaping a grain mesh on top of the picture. By comparing different size meshes and choosing the most similar, a grain size was estimated as shown on figure 3.11.

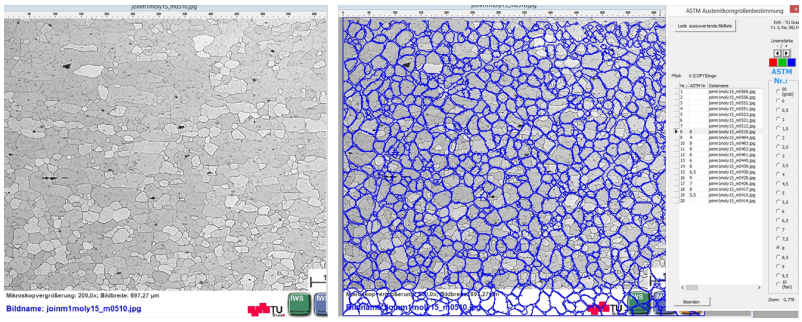

Figure 3.11: Grain size measurement procedure.

3.5.3 Hardness Measurements

Hardness tests were carried out on an automatic hardness measurement machine Emco-Test (M1C 010) along the weld with a load of 1N and a dwell time of 10 seconds. Three lines were done for each specimen on top, middle and bottom of the seam in a total of 16 measuring points per line. The indentations were spaced 0.3 mm from each other. The top and bottom lines were 0.4 mm from the top and bottom edge of the specimen respectively, while the central line was aligned with the centre of the specimen.

3.5.4 Tensile Tests

All tensile tests were carried out on a Zwick/Roell RMC 100 materials testing machine, with a test speed of 2 mm/min, at room temperature according to DIN EN ISO 6892-1 [27]. Table 3.11 lists all the tensile tests carried out in this investigation:

Table 3.11: Tensile Test Samples.

Weld	I	II	III	IV	V	VI	VII	VIII	IX	X	XI	XII
As Welded	x	x	x	x	x	x	x	x	x	x	x	x
PWHT	-	-	-	-	x	x	x	x	x	x	x	x

3.6 Summary

This chapter describes the experimental procedure adopted. However, some difficulties were faced and had to ve overcome.

The first difficulties were found related to the clamping system, and preparing a well aligned joint. When using thin plates such as the ones in this research, together with EBW with a point beam figure focused on the surface, a well aligned and secure seam is crucial to the weld final quality.

Temperature measurement is very important to further understand how the material reacts to the cooling rate and which temperatures are involved in the process. Unfortunately, measuring the temperature accurately with thermocouples, while welding, posed a challenge, since the electrons from the beam affect the measurements even when good isolation is used.

Chapter 4

Results and Discussion

This chapter presents experimental results and observations, structured in the same order as in the experimental procedure.

4.1 Bead on Plate Welding

The goal of these tests was to evaluate the depth of penetration and test the effect of the processing parameters first collected from literature research. From these results, the factor levels were set for the next experiments, in a two-factor full factorial design(FFD). Figure 4.1 shows the cross section of two welds performed.

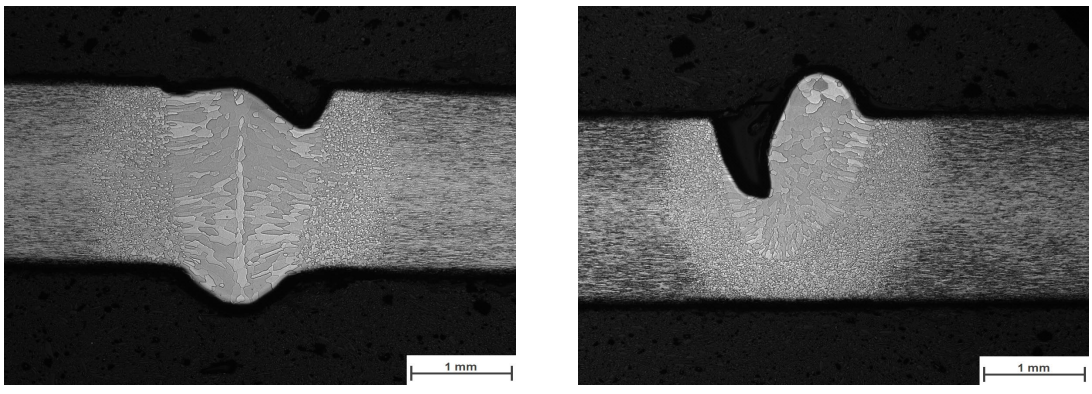

(a) (b)

Figure 4.1: Macrosections of bead on plate welds: (a) I=20 mA, v=20 mm/s; (b) I=10 mA, v=10 mm/s.

From the cross sections, it is possible to verify the coarse grains in the fusion zone (FZ), as well as the well defined heat affected zone. From the macrosection 4.1a it is clear that the fusion zone has fallen down creating a depression on the molten pool of tha face. The weld profile is not adequate neither on the face, nor on the root. On figure 4.1b, full penetration was not obtained, possibly due to the shifting of the material to the right hand side. Eventually, an interference on the magnetic field was caused, due to the clamping system.

4.2 Two-factor Full Factorial Design

To evaluate the influence and interactions of beam current and welding speed, the two-factor FFD was performed. The parameter values were a result of both literature research and the bead on plate welding test mentioned previously. From this set of welds, samples were extracted to evaluate metallographic and tensile tests. The output parameters were: width, grain size (GS) and hardness of both the fusion zone and the heat affected zone, as well as the tensile strength.

4.2.1 Macro and Microstructure

Figure 4.2 shows the cross-section of the welds. It is possible to verify that with the lower speeds undercut is present (figure 4.2a and figure 4.2b), as well as pores usually between the FZ and HAZ, with an increase in quantity and size with higher beam current (figure 4.2b). As the energy input is reduced, the weld shape improves, together with a reduction in the width of both FZ and HAZ (figure 4.2c and figure 4.2d). The smallest grain size was measured in the weld with lower energy input (I=15 mA; v=15 mm/s) in both HAZ and FZ. Table 4.1 lists the results of these output parameters. Hardness measurements and tensile tests will be discussed subsequently.

Table 4.1: Two-factor FFD results.

Weld	FZ width (mm)	HAZ width (mm)	GS-FZ (μm)	GS-HAZ (μm)
W I	1.32	1.02	52.6	20.4
W II	1.83	1.29	74.3	26.3
W III	1.12	0.64	44.2	18.6
W IV	1.23	0.68	55.9	22.5

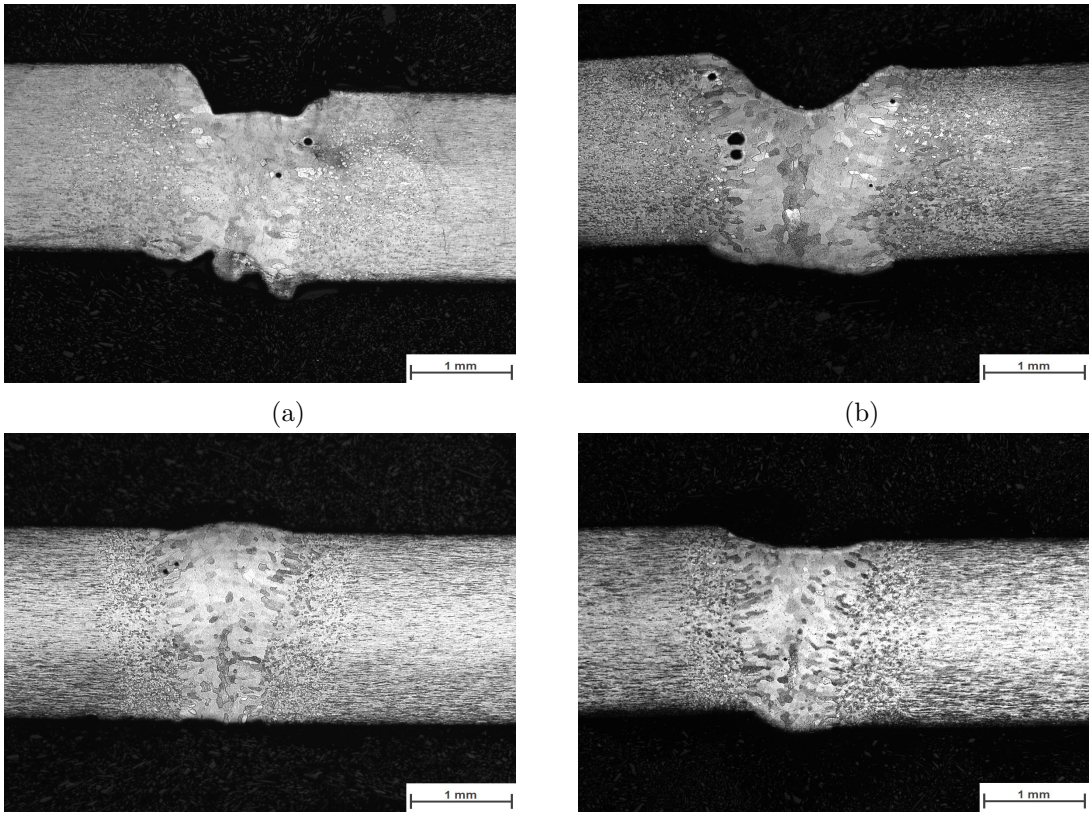

(a) (b)

(c) (d)

Figure 4.2: Macrosections of: a)I=15 mA, v=5 mm/s; b)I=25 mA, v=5 mm/s; c)I=15 mA, v=15 mm/s; d)I=25 mA, v=15 mm/s.

These results can be better understood and visualized with the charts obtained with Minitab. Figure 4.3 shows the main effect plot and the contour plot for the HAZ width. As demonstrated below, the HAZ width is mainly dependent on the variation of welding speed and the smallest HAZ is obtained with the lower beam current and higher welding speed (i.e. lower energy input).

Figure 4.4 illustrates the relationship between beam current and welding speed and their effects on the grain size of the FZ. As both parameters have a significant effect on the grain size, the contour plot allows to visualize the increase on grain size following the increase of beam current and decrease of welding speed (i.e. higher energy input). With higher energy input, a higher peak temperature is reached and a slower cooling rate is obtained, resulting in larger grain sizes.

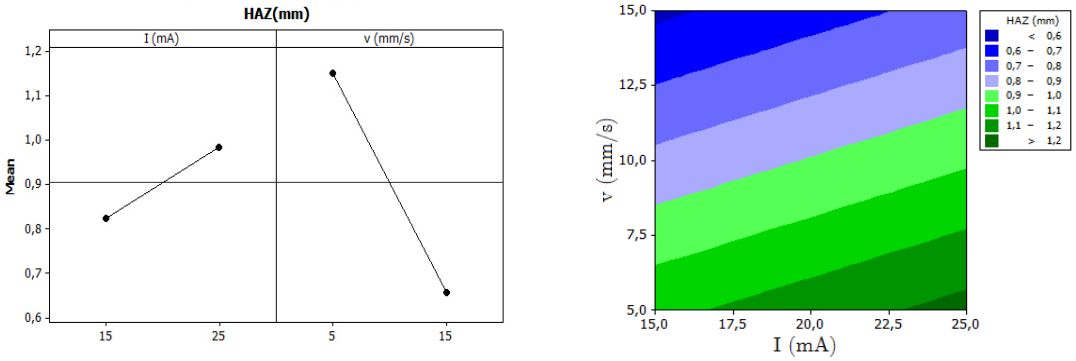

(a) (b)

Figure 4.3: HAZ width: a) Main effect plot; b) Contour plot.

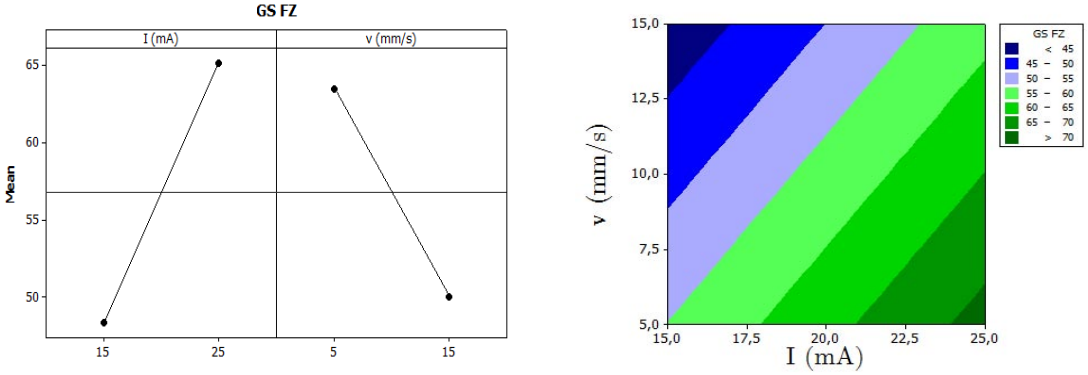

(a) (b)

Figure 4.4: Grains size of fuzion zone: a) Main effect plot; b) Contour plot.

4.2.2 Hardness of fusion zone

A macro-section with the hardness measurement indentations and a graphical representation of the hardness profile along the weld, is shown in figure 4.5. The base material shows hardness values around 290HV1 and a decrease is visible along the HAZ and FZ due to the increase in grain size.

In order to use the hardness measurements as a target variable in the FFD the average value was calculated from three measurements in each weld for the FZ and HAZ. These results are listed in table 4.2 where σ is the standard deviation.

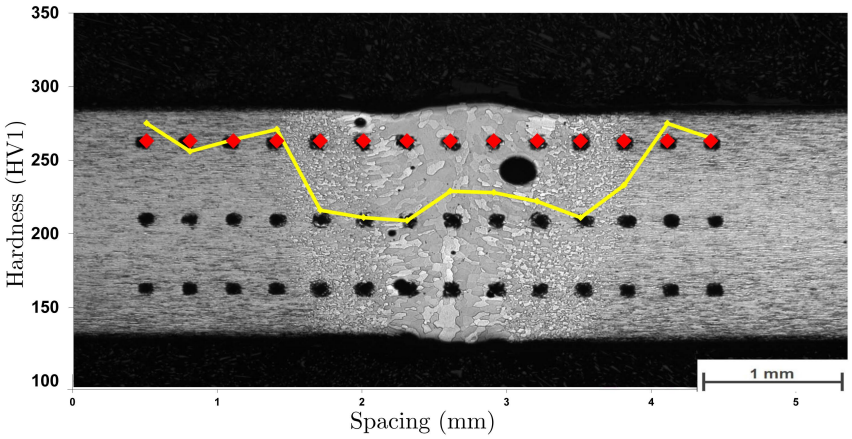

Figure 4.5: Hardness measurements in weld WIII.

Table 4.2: Average hardness values for fusion and heat affected zones.

Weld	FZ (HV1)		HAZ (HV1)	
	Avg	σ	Avg	σ
W I	199.4	11	210.5	9.7
W II	209.3	6.5	209.8	7.8
W III	222.5	6.9	222.2	9.5
W IV	221.2	7.8	219.1	10.4

Comparing the results above, there is no significant change in hardness between the samples welded with the same welding speed. However, there is an increase in hardness for the ones welded at 15 mm/s. This means that the main influence is from the welding speed while the beam current has very little effect as visible in figure 4.6a. The highest values are obtained at a higher speed of 15 mm/s as shown in the contour plot in figure 4.6b.

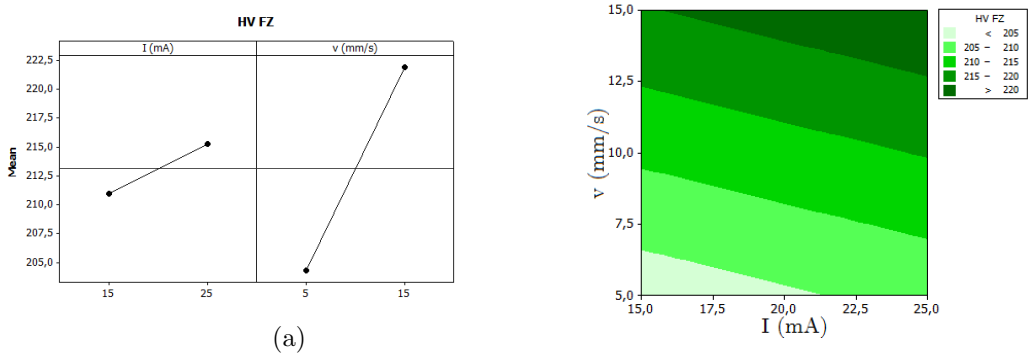

Figure 4.6: a) Main effect plot for HAZ ; b) Contour plot for HAZ.

4.2.3 Tensilte Strength

Tensile tests were conducted on samples removed from the butt welds.
Brittle fracture, predominantly by intergranular mode occurred in the fusion zone where the coarse grain formation is located as shown in figure 4.7. Table 4.3 lists the tensile test results.

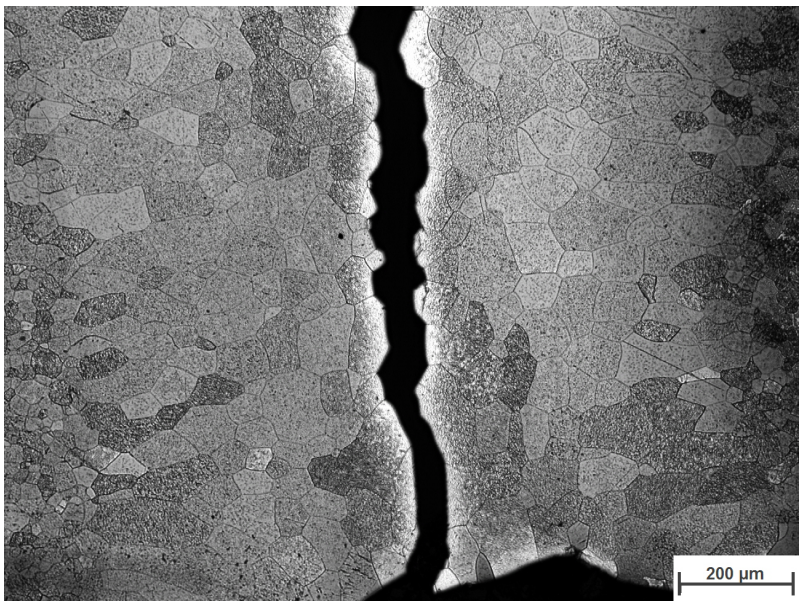

Figure 4.7: Intergranular fracture.

Table 4.3: Tensile test results.

Weld	Max. Load (kN)	Thickness (mm)	Width (mm)	UTS (MPa)
W I	24.39	2	29.5	413
W II	20.01	2	29.1	343
W III	37.82	2	29.6	638
W IV	26.60	2	30.2	440

Tensile strength values increase from 343 MPa in the weld with higher energy input, to 638 MPa in the weld with lower energy input, which surpassed the typical value of approximately 600 MPa for recrystallized TZM [2]. The significant difference between the best results is associated not only with the microstructure, but with the weld shape as well.
The two-factor FFD was conducted using the original clamping, which resulted in a misalignment os the plates as described in section 3.4.2. To avoid misalignments a new clamping system was developed as shown in figure 3.8.

4.3 Variable Welding Speed Test

From the two-factor FFD, it was understood the best results for the target variables were always obtained when welding with I=15 mA and v=15 mm/s. These welding parameters result in the lowest energy input per unit length, therefore the lower the energy input the better weld shape and mechanical properties. Before proceeding with parameter refinement, and conducting a second full factorial design, a variable welding speed test was performed.This test allowed to evaluate lower values of energy input for different beam currents and visualize their outcomes as explained in section 3.4.4. The output parameters for this welding test were the weld shape and penetration depth. Table 4.4 lists the parameters and results from these experiments.

Table 4.4: Variable welding speed test results.

Weld	HI (J/mm)	Full Penetration	Shape Quality
Dyn I	75-300	No	Not applicable
Dyn II	75-300	Yes	Bad
Dyn III	75-150	Yes	Good

Weld Dyn I was excluded, since full penetration was not obtained. Weld Dyn II revealed full penetration througout the complete welding length, proving that with lower I and energy input, compared to previous experiments in section 4.1, a butt seam weld was possible. However, the quality of the seam was poor, presenting an undercut and a variation of the weld width and shape, especially at lower speeds (figure 4.8e). Thus, 10 mA as beam current for a FFD was not desirable. Finally, weld Dyn III showed full penetration throughout the whole distance together with a good and uniform weld shape, at both lower and higher speeds (figure 4.8c and 4.8f). Although the values of energy input were as low as in Dyn I and Dyn II, increasing the beam current to 15 mA had an important role in improving the weld quality for weld Dyn III. The parameters from Dyn III were used to design the parameter window for the second FFD. Figure 4.8 shows the top view of each weld, at the higher speeds (top row) and lower speeds (bottom row).

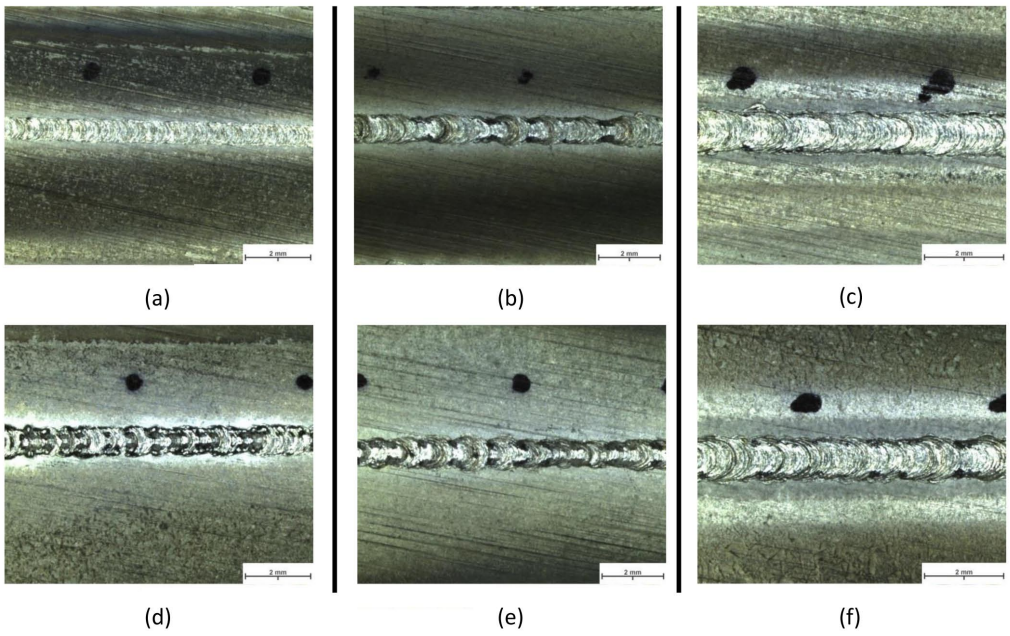

Figure 4.8: Top view at higher speed for: a)(5 mA); b)(10 mA); c)(15 mA). Top view at lower speed for: d)(5 mA); e)(10 mA); f)(15 mA).

4.4 Four-factor Full Factorial Design

The second full factorial initially considered three factors (I, v, and Preheating) at two levels. Tensile test samples were extracted in order to evaluate the effect of post-weld heat treatment in the target variables. Table 4.5 lists the four factors tested and individual effect on the target variables under analysis.

Table 4.5: Factors and target variables combination.

	HV FZ (HV1)	UTS (MPa)	GS FZ (μm)	HAZ width (mm)	Pores (μm)
I (mA)	x	x	x	x	x
v (mm/s)	x	x	x	x	x
Preheating	x	x	x	x	x
PWHT	x	x	-	-	-

4.4.1 Macro and Microstructure

From each weld, several samples for microscopy analysis were removed, in order to assess the target variables. Figure 4.9 shows the cross section of the welds and corresponding welding parameters. As in the two-factor FFD, a first observation shows different weld bead shapes resulting from the various welding parameters. Once again, associated with a higher energy input a substantial drop of the melting pool is present together with pores located between the FZ and HAZ. As the energy input is being reduced, the weld shape improves and the number of pores reduces. With the lowest energy input (75 J/mm) full penetration was obtained, with a very thin and smooth profile in both FZ and HAZ resulting from the low and highly concentrated electron beam heat input.

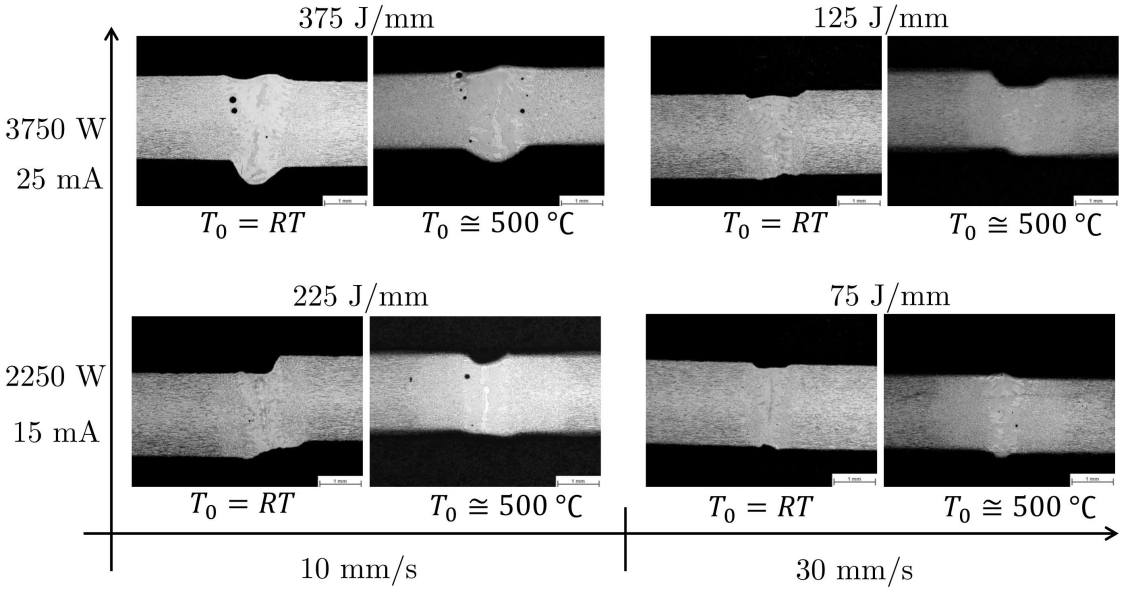

Figure 4.9: Cross section of the welds and respective parameters.

HAZ width

Measurements of the HAZ and FZ were performed. Figure 4.10 shows the measurements of welds W VII (E = 75 J/mm) and W VI (E = 375 J/mm). Both cross sections have the same magnification, which allows to visualize and compare the significant differences in size influenced by the difference in energy input. To apply the DOE procedure to the HAZ width, an average value was calculated from four measurements of each weld (weld seam top right and left, bottom right and left). Table 4.6 presents these measurments.

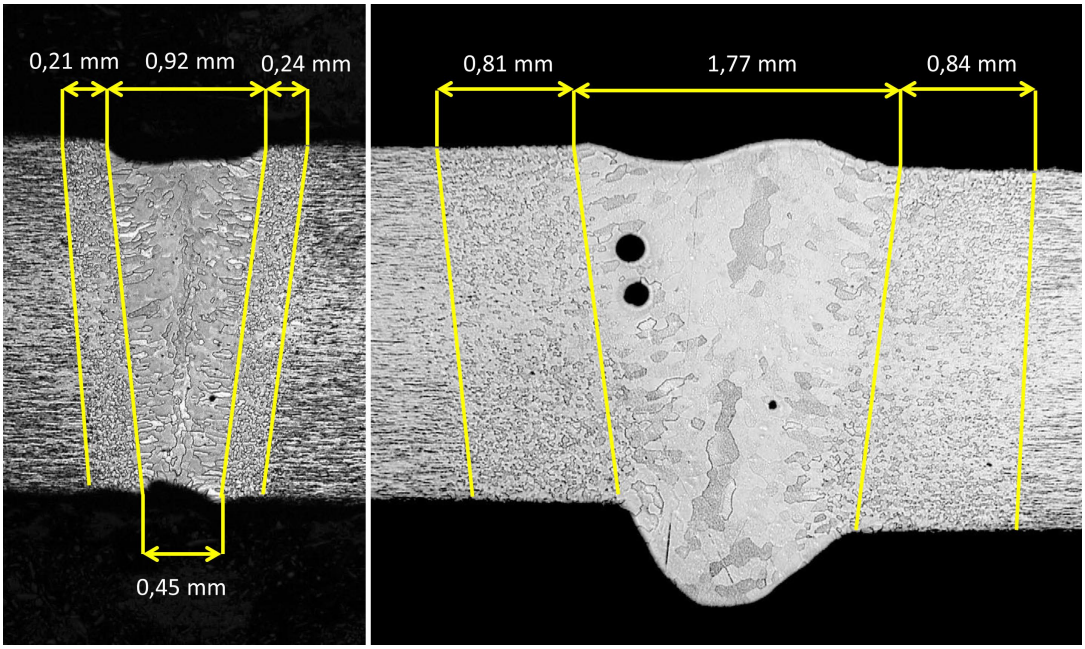

Figure 4.10: HAZ measurments for weld W VII (left) and W VI (right).

Table 4.6: Measurments of HAZ and FZ width.

Weld	HAZ (mm)	FZ (mm)
W V	0,54	1,05
W VI	0,87	1,55
W VII	0,23	0,69
W VIII	0,35	0,95
PH IX	1,14	1,21
PH X	1,97	1,75
PH XI	1,06	0,91
PH XII	0,75	1,05

The smallest HAZ was obtained with the lower values of I and v. These results are plotted in figure 4.11a. When analysing the pre-heated welds, the behaviour does not change but a general increase in the HAZ width is verified, as shown in figure 4.11b. These results are coherent with the HAZ behaviour and relationship with energy input and pre-heating temperature. The faster cooling rate from the non pre-heated and low energy input welds resulted in the smallest HAZ.

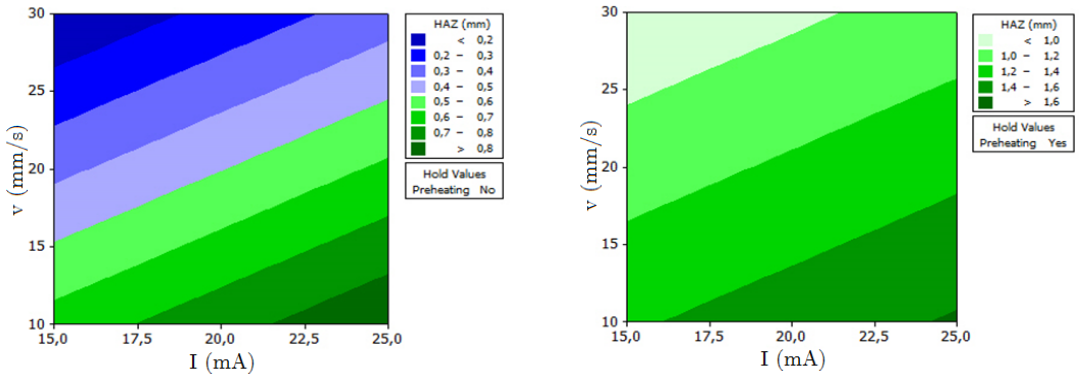

(a) (b)

Figure 4.11: Contour plots for HAZ (mm):(a)withouth PH and (b)with PH.

Grain size of fusion zone

Figure 4.12 shows the clear transition from base material (left), composed of sheet like grains typical from the roled material, into the HAZ and subsequently the FZ, where a coarse grain formation is visible, typical from the recrystallization process in Mo alloys[5]. As expected, the grains in the fusion zone are of considerable dimensions, growing from the fusion zone towards the central line with a growing direction perpendicular to the isothermal lines, typical of a material without phase transformation in solid state. In the HAZ the grain size has a gradient following the thermal gradient of the process, with small quantities of precipitates visible at grain boundaries and within the grains.

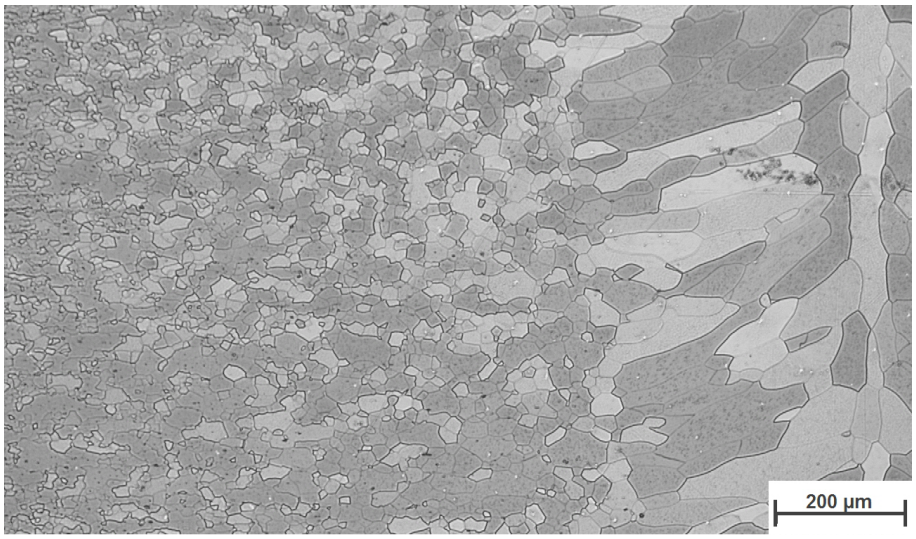

Figure 4.12: Cross section from weld PH XI.

A better visualization of the coarse grain formation in the FZ is given in figure 4.13, together with a comparison between grain sizes of HAZ and FZ at the same magnification.

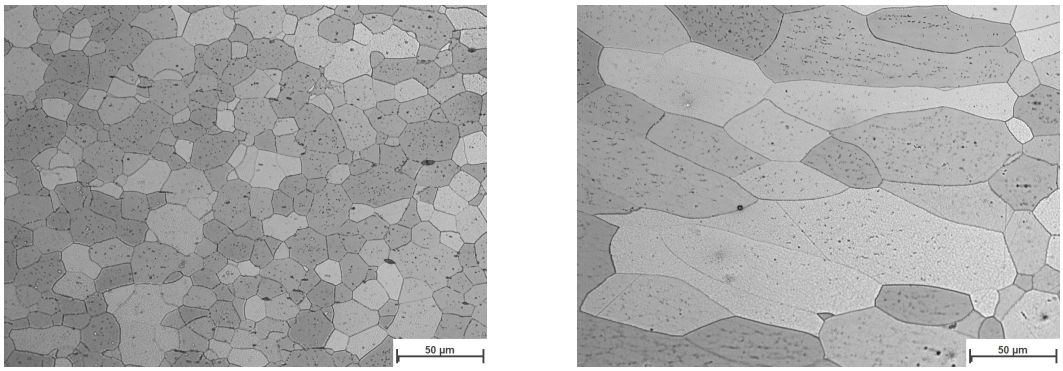

(a) (b)

Figure 4.13: Cross sections of weld PH XI: (a) HAZ ; (b) FZ.

Table 4.7 shows the results for the grain size measurements of the fusion zone.

Table 4.7: Grain size measurements in the fusion zone.

Weld	GS FZ (μm)
W V	40,7
W VI	48,4
W VII	37,8
W VIII	59,3
PH IX	53,4
PH X	81,4
PH XI	53,4
PH XII	62,5

The smaller grain sizes were obtained in the welds with lower beam current. The main influencing parameters were beam current and pre-heating, while welding speed had very little effect as shown in figure 4.14. Comparing welds W VII (I= 15mA; v= 30mm/s; RT) and PH X (I= 25mA; v= 10mm/s; PH), the grain size from the latter is more then two times bigger then the former.

The pre-heating procedure does not change this behaviour but it does contribute for a general increase in grain size in all welds, as depicted in figure 4.15b. This influence is related to the cooling rate effect on the grain growth in the FZ. Since grain growth is dependent on the magnitude and duration of the thermal cycle experienced during welding, higher power increases the magnitude while pre-heating inevitably slows down the cooling rate, allowing the grains to grow.

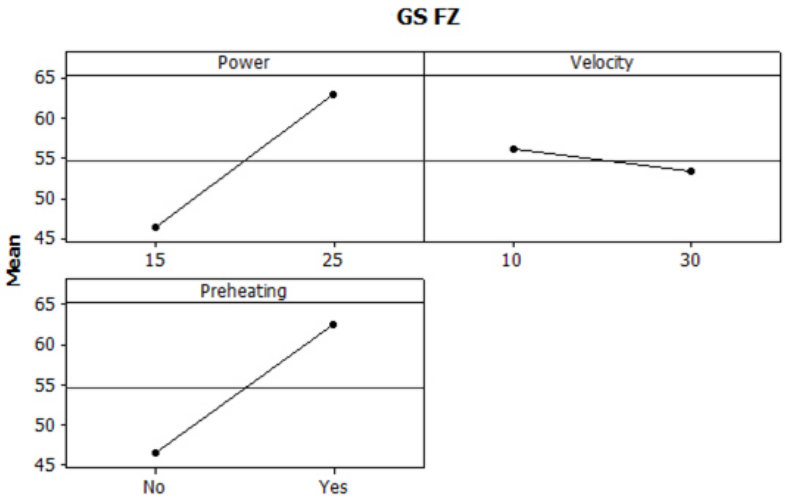

Figure 4.14: Main effect plot for grain size in FZ.

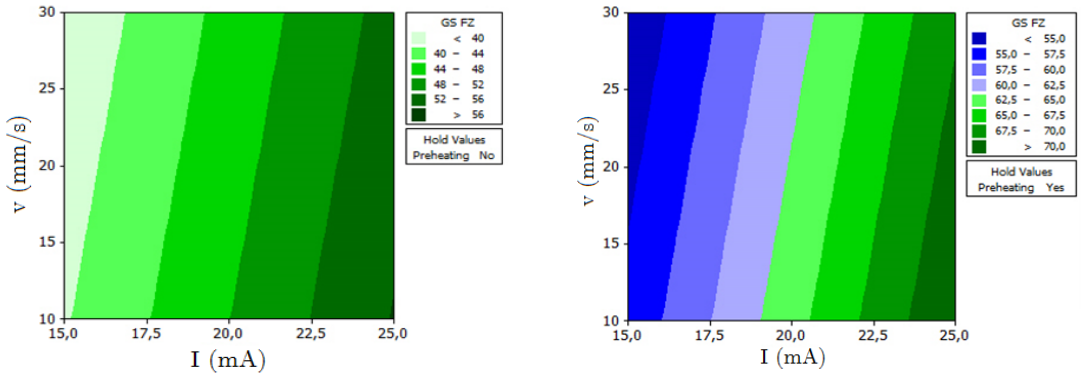

(a) (b)

Figure 4.15: Contour plots for GS FZ:(a)without PH and (b)with PH.

Pores

The table 4.8 below lists the pores counted and measured in three different specimens of each weld in order to have a representative population. The pores are organized in three different sizes, and a total number of pores is given.

Contrary to literature research [15], the results observed do not show a reduction on the number of pores in the pre-heated welds. The total number is the same between the pre-heated welds and the ones welded at room temperature. As observed in the table above, a larger quantity and size of pores is observed in the welds with higher energy input. This behaviour is observed regardless of the temperature at which welding was conducted, allowing to conclude that the number of pores is associated with the welding parameters instead of the pre-heating process.

Table 4.8: Quantity and diameter of pores.

Weld	Small ($d \leq 50\,\mu m$)	Medium ($50\,\mu m < d < 100\,\mu m$)	Big ($d \geq 100\,\mu m$)	Total Pores
W V	4	1	0	5
W VI	6	3	2	11
W VII	1	1	0	2
W VIII	4	1	1	6
PH IX	5	3	3	11
PH X	2	3	3	8
PH XI	1	1	0	2
PH XII	3	0	0	3

X-ray photographs were obtained from each weld, at PLANSEE. Figure 4.16 shows the comparison between welds W VIII and PH X, which respectively represent a room-temperature weld with low energy input and a pre-heated weld with high energy input. It is clearly visible, several pores along the weld seam in weld PH X and only one pore in weld W VIII.

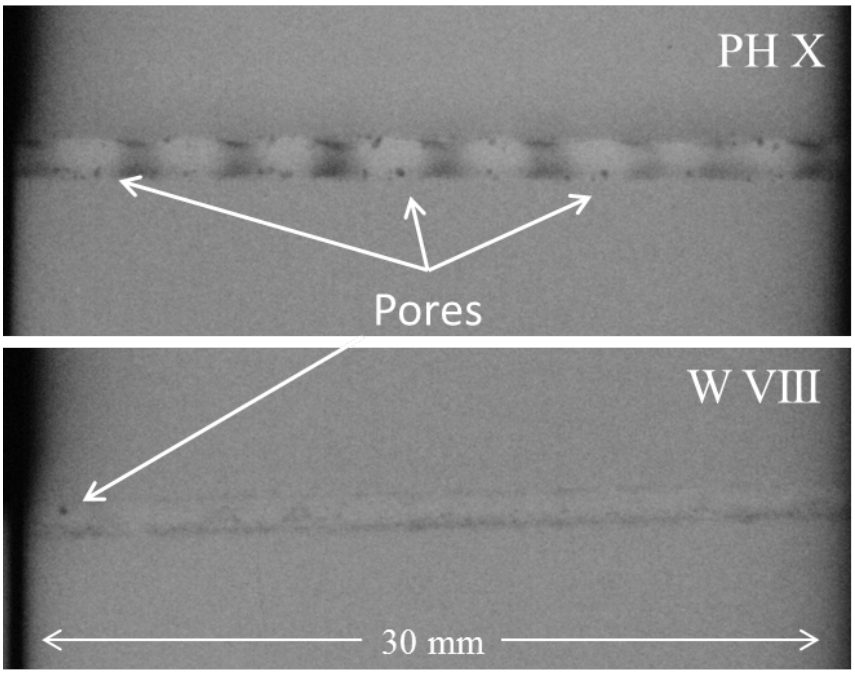

Figure 4.16: X-ray photos of weld PH X (top), and W VIII (bottom).

By multiplying the number of pores by their size, the target variable *Porosity* was created and applied in the FFD as seen in figure 4.17. The occurrence of pores is probably associated with the instability of the keyhole during the welding process, leading to entrapped gases. Welding speed is the main influencing parameter because an unfavourable selection of this welding parameter results in metal fumes not escaping from the keyhole which, upon cooling, leads to pores. This can be supported by looking closer at figure 4.16. The pores are systematically located at the border of the fuzion zone and follow the weld bead wavy pattern that resulted from the high beam current and low welding speed.

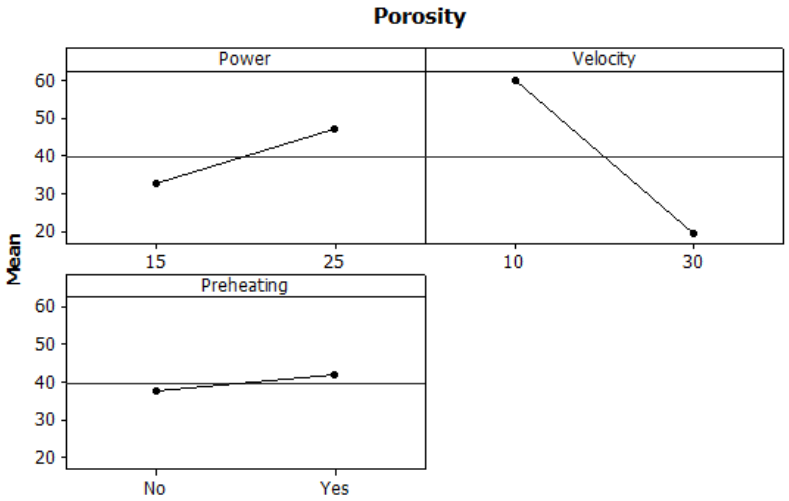

Figure 4.17: Main effect plot for porosity.

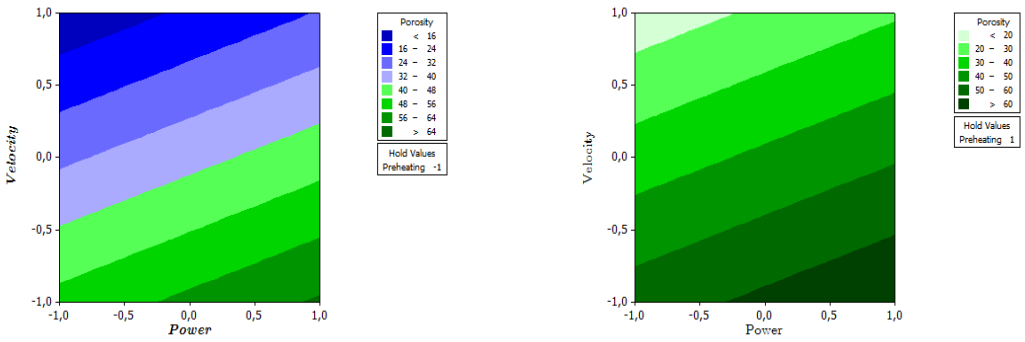

(a) (b)

Figure 4.18: Contour plots for Porosity:(a)without PH and (b)with PH.

4.4.2 Hardness of Fusion zone

Following the same procedure as in section 4.2.2, three lines of indentations were made on each weld. Figure 4.19 shows the location of the indentations together with the hardness profiles. A regular behaviour is visible when comparing the three profiles.

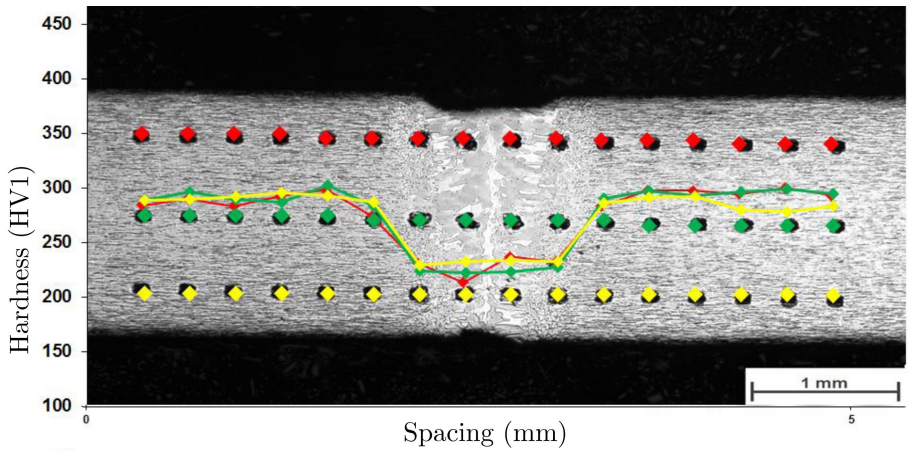

Figure 4.19: Hardness profiles in weld W VII.

By calculating the average of the three profiles and plotting the results from the welds together, it is possible to verify the difference in hardness between welds. Figure 4.20 illustrates hardness measurement profiles for different welds. The base material shows hardness values of around 290HV1 and a sharp drop occurs when the HAZ starts and continues to the FZ. The hardness values of FZ vary between 230HV1 and 200HV1. Figure 4.20 also shows the different HAZ widths interpreted from the hardness profiles.

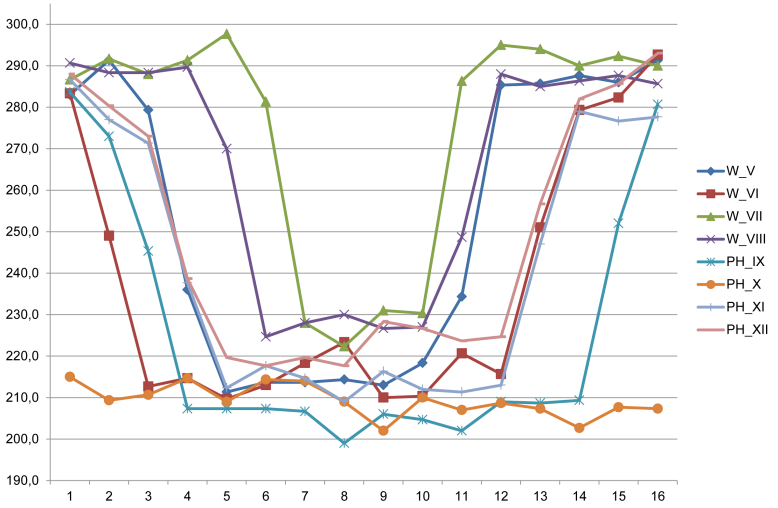

Figure 4.20: Hardness profiles from the welds.

Table 4.9 shows the results from the hardness measurements of the fusion zone, average values (Avg), maximum values (Max) and standard deviation (σ). Hardness testing was conducted in the specimens after the stress relieving procedure, allowing this target variable to be associated with the four parameters.
The relevant parameters are shown in figure 4.21 with the highest influence attributed to pre-heating, followed by welding speed and PWHT. Pre-heating and PWHT contributed to a decrease in the hardness of the FZ, while increasing the speed resulted in higher hardness values. The highest maximum value of 244 HV1 was obtained from specimen TT-W VIII and the highest average value of 227 HV1 was obtained in weld W VII. In general, the welds with I = 25 mA and v = 30 mm/s registered the highest results.

Table 4.9: Hardness values of the fusion zone.

	Hardness of fusion zone		
Specimen	Max	Avg	σ
W V	220	214	7
W VI	230	219	5.8
W VII	237	227	7.1
W VIII	230	225	6.6
PH IX	211	204	5.4
PH X	224	204	9.2
PH XI	222	213	5.1
PH XII	230	223	5.6
TT-W V	218	213	8.2
TT-W VI	235	216	14.4
TT-W VII	225	211	12.5
TT-W VIII	244	223	17.8
TT-PH IX	207	200	6.4
TT-PH X	212	200	6
TT-PH XI	220	207	13
TT-PH XII	230	208	8.7

These results are confirmed in figure 4.22 which shows the contour plots for HV in the FZ with and without PH and PWHT. By comparing both contour plots, a reduction in hardness values is observed when pre-heating and PWHT are introduced. In figure 4.22b the general behaviour of results changes slightly at lower speeds but the highest HV values are still occurring at the higher welding speed. Nevertheless, the influencing parameters tested (I, v) which control the energy input, mainly affect the extend of both FZ and HAZ, and do not have a significant influence in the hardness of these zones, since there is no solid state transformation, but a homogeneous distribution of the very small precipitates within the grains.

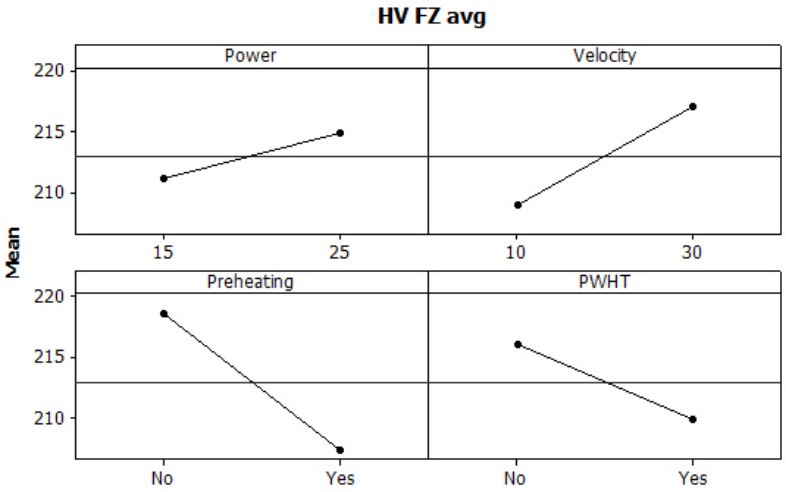

Figure 4.21: Main effect plot for average HV in FZ.

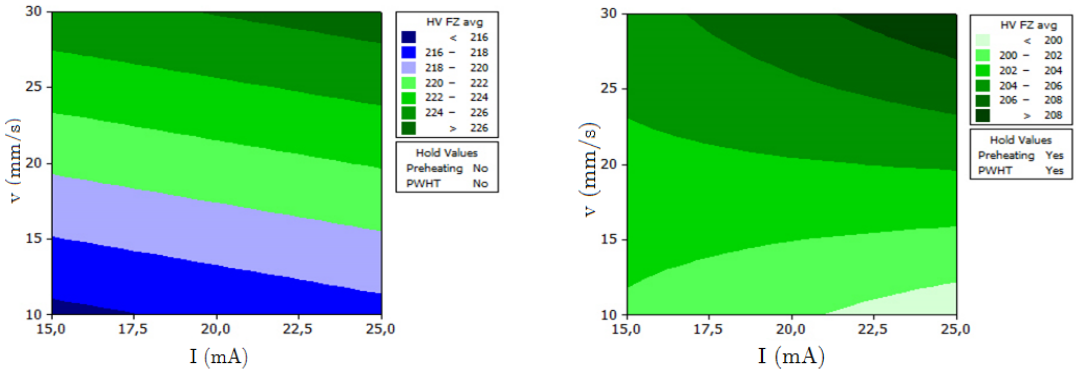

(a) (b)

Figure 4.22: Contour plots for HV FZ: (a) withouth and (b) with PH and PWHT.

From the contour plots above, it is clear that beam current has almost no effect on the hardness of the FZ, while welding speed plays the major role.

4.4.3 Tensile Stregth

Tensile tests were conducted as welded and after the PWHT. This set of tests allowed to re-evaluate the role of I and v in the mechanical properties of the weld, as well as to verify if PWHT improves the mechanical properties[7]. A base material tensile test was conducted for comparison. Table 4.10 shows the measured values for the tensile tests conducted as welded, together with the base material sample (BM).

Table 4.10: Tensile test results of BM and as welded samples.

Sample	Max. Load (kN)	Thickness (mm)	Width (mm)	UTS (MPa)
BM	51.67	2	30	861.0
W V	26.66	2	29.4	453.4
W VI	28.09	2	30.3	477.7
W VII	40.96	2	30.6	669.2
W VIII	39.95	2	30	665.8
W IX	23.59	2	29.7	397.1
W X	23.04	2	29.7	387.2
W XI	21.08	2	20	527.0
W XII	31.26	2	30.05	520.1

The base material showed a tensile strength of 861 MPa. Most welds registered values in the range of 50% of the base material strength, but welds W VII and W VIII (both with v = 30 mm/s and no pre-heating) showed improved results of approximately 77% of the base material tensile strength. These values are approximately 10% above the recrystallized TZM tensile strength of 600 MPa [2]. All welds revealed the typical behaviour of a coarse grain material, with brittle fracture that occurred along the FZ centreline as shown on figure 4.23.

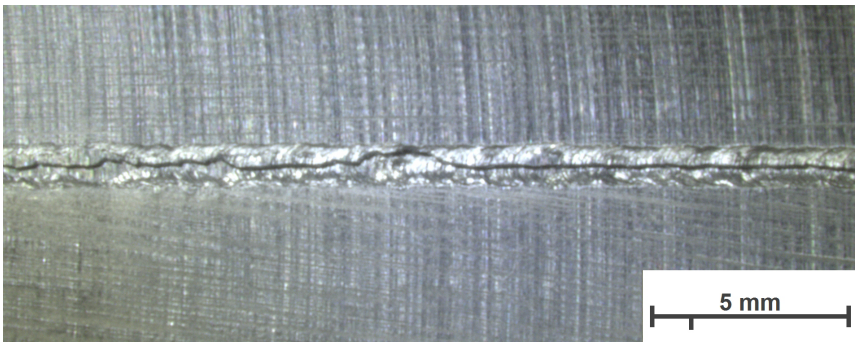

Figure 4.23: Crack along the fusion zone in weld VII (I= 15mA, v= 30mm/s).

The results of the stress relieved tensile specimens are listed in table 4.11.

Table 4.11: Tensile test results of stress relieved specimens.

Weld	Fm (kN)	Thickness (mm)	Length (mm)	UTS (MPa)
W V	29.49	2	30.08	490.2
W VI	29.38	2	30.28	485.1
W VII	39.05	2	30.17	647.2
W VIII	36.83	2	30.2	609.8
W IX	21.77	2	29.52	368.7
W X	20.88	2	29.66	352.0
W XI	14.96	2	19.66	380.5
W XII	27.22	2	29.86	455.8

Specimens PWHT-WV and PWHT-WVI show a slight increase in UTS, between 10% to 3,5% respectively, compared to their corresponding specimen tested as welded. For the remaining welds a slight decrease is observed. The general behaviour of results was not altered with the introduction of a PWHT. The highest values were again obtained from welds W VII and W VIII with the main influencing parameter being welding speed as shown in figure 4.24.

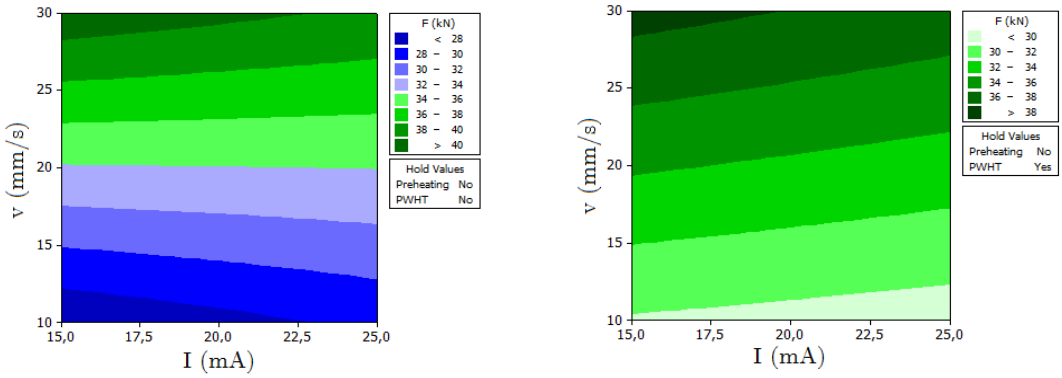

(a) (b)

Figure 4.24: Contour plots for Force (kN):(a)withouth PWHT and (b)with PWHT.

Opposed to what was observed previously in figure 4.7, a predominantly transgranular cracking was present, as shown in figure 4.25.

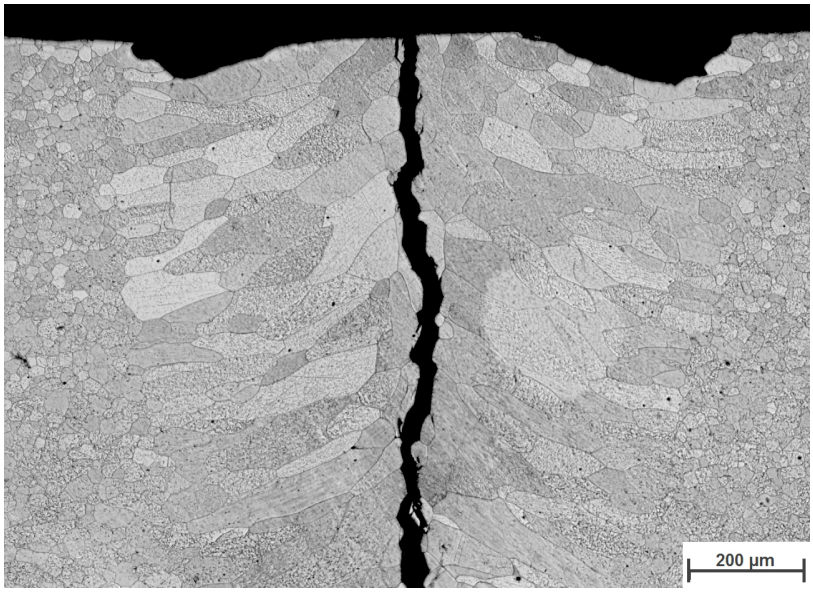

Figure 4.25: Transgranular fracture in weld XI after PWHT.

4.5 Summary of results

Through the application of design of experiments, it is shown that with careful selection and refinement of the welding parameters it is possible to considerably reduce the size of the heat affected zone and the grain size of the weld. Still, a coarse grain formation was always present in the fusion zone together with a hardness reduction since this Mo alloy has no solid state transformation. Electron beam welding proved to be a reliable and well reproducible process. The correctly selected parameters resulted in high quality, pore free welds, but brittle fracture was not eliminated. Finally, pre- and post-weld-treatment processes do not effect the welding results of these experiments significantly.

Chapter 5

Conclusions and Future Work

5.1 Conclusions

From the study performed the following conclusions can be drawn:

- Successful joints free of defects were produced in TZM by electron beam under appropriate processing conditions.
- The design of experiments methodology allowed to identify the best window of parameters, their influence on pre identified target variables and interactions between these.
- For the maximum accelerating voltage, lowering the beam current and increasing the welding speed, that is, lowering the welding heat input produced systematically the best welds. The best operating parameters tested were of: 75 J/mm, 15 mA and 30 mm/s.
- A coarse grain structure was always seen in the fusion zone, with a grain size larger then 37.8 μm which was obtained at the minimum heat input.
- The HAZ was measured, and is directly proportional to energy input per unit length. The smallest HAZ (0,23 mm) was obtained in weld W VII (I = 15 mA, v = 30 mm/s) and I and v play both an important role in affecting the HAZ width, with pre-heating contributing to a slower cooling rate, resulting in a general increase of HAZ width.
- A reduced number of pores was seen with dimensions below 50 μm, especially located in the fusion line, and thus porosity can be neglected. Nevertheless welding speed was seen as the main influencing parameter as far as porosity is concerned.

- Hardness values in the FZ were of about 227HV1 for the welds with lowest energy input. This corresponds to a drop of about 70HV1 compared to the base material. No hardness peaks were observed in the HAZ.
- Tensile tests of the welds showed a maximum of 77% of the base material UTS, in the welds with the lowest heat input.
- Fracture always occured along the FZ in the centreline in an intergranular fracture mode.
- Neither the preheating nor the post weld heat treatment were seen to affect the properties of the welds. So the PWHT performed by the company should not be conducted, with a reduction in production costs.

5.2 Future Work

Concerning the electron beam welding process, from the parameters kept constant in this research, focal point and beam oscillation could be of interest in further investigations. Furthermore, exploring other possibilities available from EBW could be done, such as a two passage weld, or a multi pool welding passage. These procedures would contribute to increase the number of solid nuclei and thus reduce the grain coalescence. Another experiment, would be to apply a multi process technique, where beam deflection creates two heating zones parallel to the weld seam while simultaneously welding the joint.
One of the most important factor in the mechanical properties and improving ductility of Mo based alloy welds, is the distribution and content of interstitial elements, especially at grain boundaries. Energy-dispersive X-ray spectroscopy would allow to investigate these characteristics and correlate with the welding parameters.
Applying a thermal cycle to the welded specimens, identical to the real industrial application to verify consequences, changes in the micro-structure and mechanical properties of the welds.

Bibliography

[1] J Shields. *Applications of Molybdenum Metal and its Alloys*. ed. Int. Molybdenum Association, Munich, 2013.

[2] PLANSEE SE. Info-booklet molybdenum material properties and applications, 2013.

[3] AJ Bryhan. Joining of molybdenum base metals and factors which influence ductility. Technical report, Exxon Production Research Co., Houston, TX, 1986.

[4] EM Savitskii and GS Burkhanov. *Physical metallurgy of refractory metals and alloys*. ed. Springer US, Boston, MA, 1970.

[5] Jiteng Wang, Juan Wang, Yajiang Li, and Deshuang Zheng. Progress of research on welding for molybdenum alloys. *High Temperature Materials and Processes*, 33(3):193–200, 2014.

[6] Yutaka Hiraoka, Masatoshi Okada, and Hirosada Irie. Alloying to improve the properties of welded molybdenum. *Journal of Nuclear Materials*, 155:381–385, 1988.

[7] Fumio Morito. Tensile properties and microstructures of electron beam welded molybdenum and tzm. *Journal of the Less Common Metals*, 146:337–346, 1989.

[8] S Majumdar, S Raveendra, I Samajdar, P Bhargava, and IG Sharma. Densification and grain growth during isothermal sintering of Mo and mechanically alloyed Mo–TZM. *Acta Materialia*, 57(14):4158–4168, 2009.

[9] Jinglian Fan, Mingyuan Lu, Huichao Cheng, Jiamin Tian, and Boyun Huang. Effect of alloying elements Ti, Zr on the property and microstructure of molybdenum. *International Journal of Refractory Metals and Hard Materials*, 27(1):78–82, 2009.

[10] Masahiro Nagae, Tetsuo Yoshio, Jun Takada, and Yutaka Hiraoka. Improvement in recrystallization temperature and mechanical properties of a commercial tzm alloy through microstructure control by multi-step internal nitriding. *Materials transactions*, 46(10):2129–2134, 2005.

[11] W Behr and U Reisgen. Innovatives elektronenstrahlschweißen hochschmelzender metalle. *Materialwissenschaft und Werkstofftechnik*, 38(7):504–509, 2007.

[12] Fumio Morito. Effect of impurities on the weldability of powder metallurgy, electron-beam melted and arc-melted molybdenum and its alloys. *Journal of Materials Science*, 24(9):3403–3410, 1989.

[13] Rudolf Lison. *Schweißen und Löten von Sondermetallen und ihren Legierungen.* Dt. Verlag für Schweißtechnik, DVS-Verlag, 1996.

[14] BV Cockeram, Evan Keith Ohriner, Thak Sang Byun, MK Miller, and LL Snead. Weldable ductile molybdenum alloy development. *Journal of Nuclear Materials*, 382(2):229–241, 2008.

[15] B Tabernig and N Reheis. Joining of molybdenum and its application. *International Journal of Refractory Metals and Hard Materials*, 28(6):728–733, 2010.

[16] K. Ladislav M. Kolarikova and P. Vondrous. Welding of thin molybdenum sheets by ebw and gtaw. *Proceedings of the 23rd International DAAAM Symposium*, 23(1):1005–1008, 2012.

[17] Daniel de Pretis. Friction welding of TZM components. Master's thesis, Graz University of Technology, 2014.

[18] D. Dobeneck T. Krssel T. Lwer V. Adam, U. Clau. *Electron Beam Welding - The fundamentals of a fascinating technology.* ed. pro-beam AG & Co. KGaA, Burg, Germany, 2011.

[19] Helmut Schultz. *Electron beam welding.* ed. Elsevier, 1994.

[20] Stanislaw Gratkowski, Andrzej Brykalski, Ryszard Sikora, Marek Ziolkowski, and Hartmut Brauer. Modelling of seebeck effect in electron beam deep welding of dissimilar metals. *COMPEL-The international journal for computation and mathematics in electrical and electronic engineering*, 28(1):140–153, 2009.

[21] Christopher Wiednig. Electron beam welding alloy 625. Master's thesis, Graz University of Technology, 2013.

[22] G. Schubert. Electron beam welding: Process, applications and equipment. Accessed: 2015-07-26.

[23] Douglas C Montgomery. *Design and Analysis of Experiments*, volume 8. John Wiley & Sons New York, 2012.

[24] Mathias Dobner. *Untersuchungen zum Elektronenstrahlschweissen dickwandiger Bauteile*. Shaker, 1997.

[25] Markus Stutz. Surface structuring of biodegradable mg-alloys by electron beam technique. Master's thesis, Graz University of Technology, 2014.

[26] Josef Pfeifer. Vorwrmen von bauteilen mittels elektronenstrahl. Bachelor's thesis, Graz University of Technology, 2014.

[27] ISO. Metallic materials - Tensile Testing - Part 1: Method of test at room temperature. ISO, International Organization for Standardization, Geneva, Switzerland, 2009.

Appendix A

New clamping technical drawing

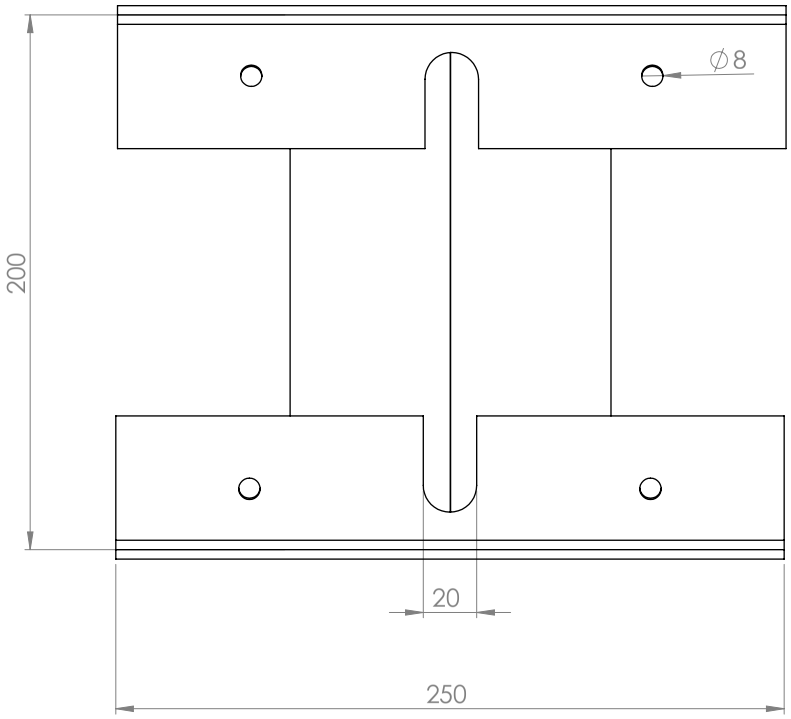

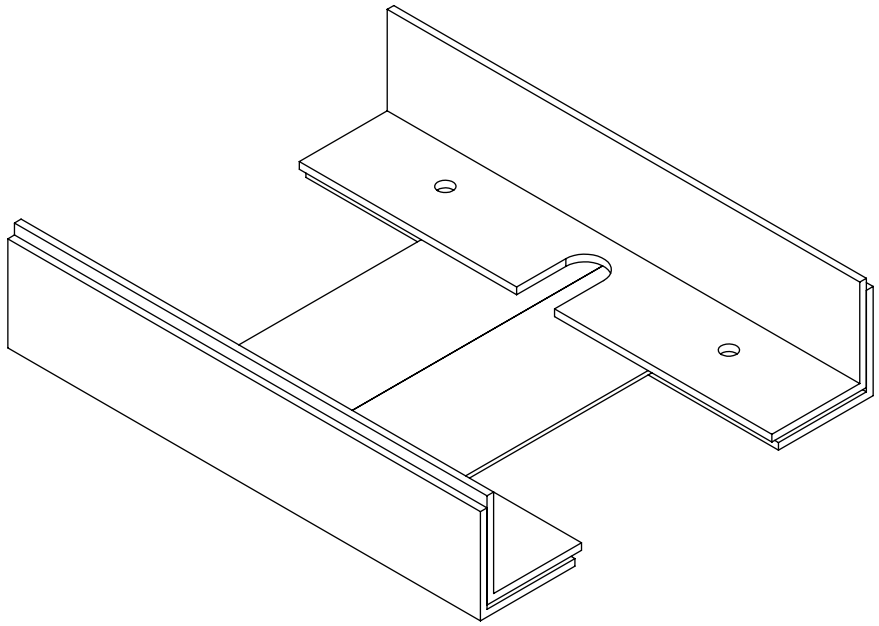

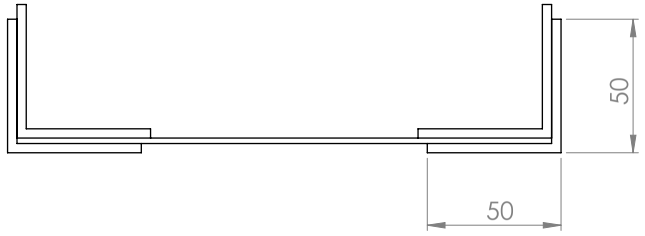

UNLESS OTHERWISE SPECIFIED: DIMENSIONS ARE IN MILLIMETERS SURFACE FINISH: TOLERANCES: LINEAR: ANGULAR:		FINISH:		DEBUR AND BREAK SHARP EDGES	DO NOT SCALE DRAWING	REVISION
	NAME	SIGNATURE	DATE		TITLE:	
DRAWN						
CHK'D						
APPV'D						
MFG						
Q.A				MATERIAL:	DWG NO. clamping final2	A3
				WEIGHT:	SCALE:1:2	SHEET 1 OF 1